Flux pinning

C. J. van Der Beek, P. H. Kes

A3.2
Flux pinning

C J van der Beek and P H Kes

A3.2.1 Introduction

Type II superconductors with high upper critical fields H_{c2} have considerable potential for practical applications, including high magnetic field solenoids, permanent magnets and energy storage devices, as well as magnetic field detectors (SQUID's) and superconducting components for electronics and communications. However, the interplay between electrical currents and lines of quantised magnetic flux (the "flux lines", "vortex lines", or simply "vortices" of Section A.~~2.3.3~~), in superconducting materials results in a driving force that puts the latter in motion. Vortex motion leads to dissipation of energy, manifested as an electric potential within the material, which therefore can no longer be considered to be superconducting, i.e. its electrical resistance becomes non-zero [Bardeen and Stephen 1965]. Preventing vortex motion up to a high critical current density j_c is therefore essential. This is achieved through *pinning* of the vortex lines by imperfections of the material. Fortunately, such flux pinning is a general phenomenon in commonly produced materials. In the following sections an overview is given of this interesting phenomenon and some related issues.

A3.2.2 Origin of flux pinning : material defects and flux pinning interactions

Material imperfections providing flux pinning occur in many different varieties, and include inhomogeneities, defects, and engineered structures of sizes ranging from the atomic scale to the macroscopic. They are either naturally present as a result of the composition of the material, artificially introduced as the byproduct of the growth or preparation method, or tailored by micro- or nano-engineering. It is safe to assume that any imperfection of the material will lead to some extent of flux pinning and therefore affect the macroscopic physical properties of the superconductor, even if the effects may be very small. However, for the vast majority of superconducting materials, including technological superconductors, flux pinning will completely determine the electrical transport and magnetic properties in the superconducting state. One may classify flux pinning defects through the origin of the interaction with the vortex lines, through their "strength", and through their shape: a cylindrical defect extending along the length of a vortex line will generally be more effective in arresting it than a point-like imperfection.

Imperfections locally alter material properties and, consequently, superconductivity in their environment. Such changes couple to the periodic variations of both the order parameter and the local electromagnetic field, which are characteristic of the mixed state (see chapter A~~4.2~~). In principle the interaction can be derived by solving the Ginzburg–Landau equations with the appropriate boundary conditions imposed by the defects. Most commonly, the vortex-defect interaction force $f(r)$ is attrac-

tive, so that the presence of imperfections results in a random "landscape" $U_{pin}(\mathbf{r})$ of attractive pinning potential wells for the vortices. However, repulsive pins also exist. An example of such are engineered magnetic centres (see *e.g.* [Marchiori *et al.* 2017]) of polarity equal to that of the vortices.

A3.2.2.1 The core interaction

The local modification of the order parameter (related to the density of Cooper pairs) by the presence of defects has an incidence on the electronic structure and the diameter of the vortex core. One therefore speaks of "core pinning". Defects deviate from the surrounding material by differences in density, elasticity, or electron-phonon coupling. These give rise to a local change in T_c – and hence of the condensation energy $\frac{1}{2}\mu_0 H_c^2$ – which may range from a minor, secondary effect (due to local strain, for example) to the complete suppression of superconductivity in or around the defect. The defects may also manifest themselves through their scattering effect on quasiparticles in the vortex core, and the subsequent changes in quasiparticle mean free path ℓ, quasi-particle conductivity and vortex core level structure. One thus distinguishes between δT_c– and $\delta\ell$–pinning.

The coupling to the variation of the order parameter is the main origin of flux pinning by very many types of defects, including dislocations, point defects of various kinds, voids, grain boundaries, precipitates, and ion-irradiation induced damage such as amorphous columnar defects. The typical length scale r_f of the core interaction depends on the spatial variations of the order parameter. Therefore, $r_f \approx \xi$ for low ($B < 0.2B_{c2}$) and $r_f \approx a_0/2$ for high flux densities respectively, where a_0 is the vortex lattice parameter ($\frac{1}{2}a_0^2\sqrt{3} = \Phi_0/B \equiv n_v$ is the vortex line areal density). The elementary pinning force $f(u)$ generally assumes its maximum value f_p for a vortex displacement $u \approx r_f$.

A3.2.2.2 The electromagnetic interaction

Imperfections of size comparable to or larger than the London penetration depth λ_L (see Eq. (A2.2.4)) will necessarily alter the supercurrent flow in the material, including that of vortex currents. The associated spatially-dependent reduction in the kinetic energy provides the attractive pinning interaction. Examples of the magnetic interaction are the attraction of vortex lines to surfaces parallel to the applied magnetic field H_a (this might be the external surface, see section *A3.2.3.6*, as well as some large precipitate interface within the sample bulk) and thickness variations of thin films for fields normal to the film. In the latter case, the vortices are trapped at the sites of least thickness where the line energy of the vortex is minimum.

Evidently, the typical length scale related to the magnetic interaction is λ. In materials with a large κ this kind of interaction is therefore relatively small; also it rapidly vanishes as the magnetic field increases beyond several H_{c1}. The electromagnetic interaction with large defects and the surface can be readily modelled using the image vortex method [Clem 1974]. A secondary effect of small defects is the depletion of the Cooper pair (superfluid) density, which may entail a spatially modulated increase of λ. Inhomogeneities of the defect distribution will therefore contribute to flux pinning, with vortices being attracted to regions of larger average λ [Demirdis *et al.* 2013].

A3.2.3 Effect on electromagnetic and transport properties in the mixed state

A3.2.3.1 Electric conductivity and the $E(j)$ relation

Experimentally, flux pinning manifests itself in many ways which provide one with different opportunities to measure the critical current density j_c. Given that the local current density $\mathbf{j}$ is proportional to the force $\mathbf{F}_L = \mathbf{j} \times \mathbf{B}$ on the vortices, and the electric field $\mathbf{E} = \mathbf{v} \times \mathbf{B}$ (averaged over a distance larger than several times a_0) is given by the cross product of average vortex velocity $\mathbf{v}$ and the flux density $\mathbf{B}$, the local relation between electric field and current density $E(j)$ reflects the average force-velocity curve characterising the motion of the vortices through the pinning "landscape". Ideally, $|\mathbf{E}| = |\mathbf{v}| = 0$ up

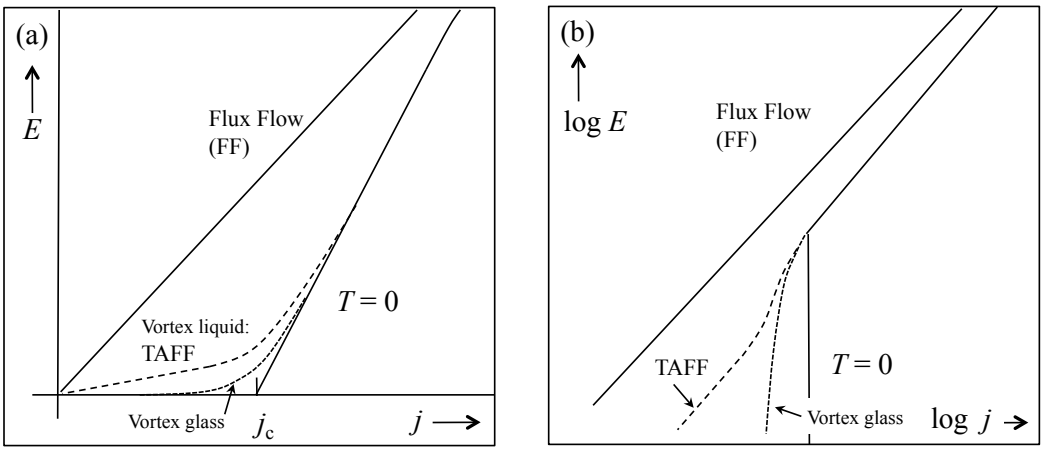

Figure A3.2.1: Typical $E(j)$ characteristics in the mixed state in the absence of pinning (FF), with bulk pinning at zero temperature ($T = 0$) and at finite temperature for finite energy barriers (TAFF, dashed, appropriate for the vortex liquid phase) and infinite barriers (glass, dotted) for $j \to 0$, rendered as a linear (a) and double logarithmic plot (b). Note that the differential resistivity above the critical current density j_c is larger than or equal to the flux flow (FF) resistivity in the absence of pinning. This effect is due to velocity fluctuations and is more than often ignored.

to $|\mathbf{j}| = j_c$ and then rises almost linearly, with a slope slightly greater than the flux flow resistivity ρ_f for $j > j_c$ (see below and figure A3.2.1). Thus $j_c \equiv F_p/B$ is defined as the critical current density that will overcome the net "volume" pinning force F_p (unit [N/m^3]) exerted by the material imperfections on the vortex ensemble, thereby setting the latter in motion. A reasonable approximation for ρ_f is $\rho_f \approx \rho_n(B/B_{c2})$ [Bardeen and Stephen 1965], where ρ_n is the electrical resistivity in the normal state, suggesting that the dissipation takes place mainly in the core of the moving flux lines. In strong pinning materials j_c can be as large as a few tenths of the depairing current density, $j_0 \approx H_c/\lambda$ (see Section A2.2), which is typically 10^8 A/cm^2. To achieve such large current densities in electrical transport measurements is difficult due to heating effects and contact problems, and therefore inductive probes (magnetic measurements) are frequently used.

A3.2.3.2 Inductive measurements and magnetic hysteresis

In the absence of pinning centres, surface or geometrical effects, the flux distribution inside a superconductor in a magnetic field $H > H_{c1}$ is uniform with density B. The Meissner screening currents in a surface layer of thickness λ produce a (diamagnetic) moment m and an associated volume magnetisation M which is in equilibrium with H, as described by the reversible magnetisation curve of Abrikosov (see chapter A4.2), i.e. $M = M_{rev}(H)$ and $B_{rev}(H) = \mu_0(H + M_{rev})$ [Indenbom *et al.* 1994].

Since their electromagnetic response is dictated by their nonlinear $E(j)$ curve rather than by the London equation, type-II superconductors with flux pinning in the material bulk behave as perfect conductors rather than superconductors. Their response to low-frequency time-varying electromagnetic fields is described by a set of macroscopic nonlinear diffusion equations for the (electro-)magnetic field and the

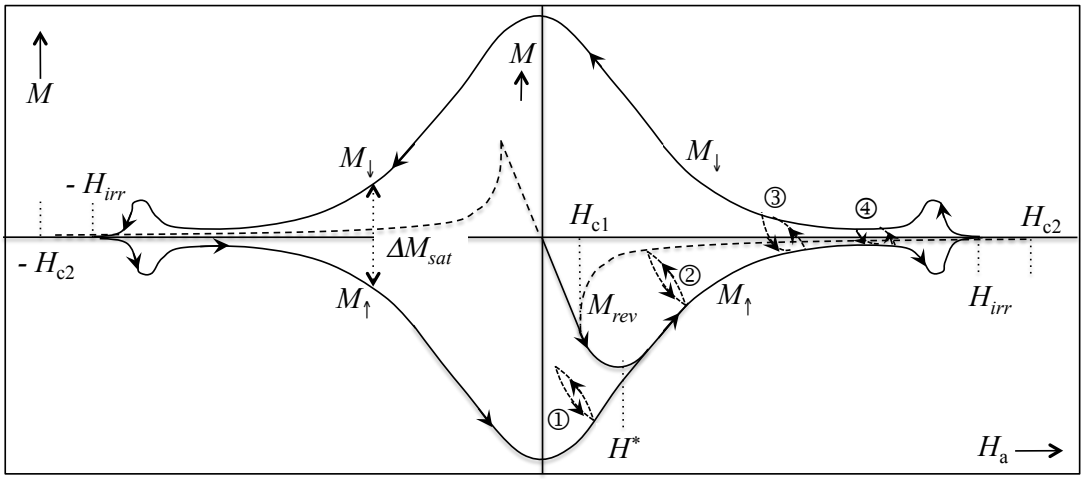

Figure A3.2.2: Model magnetisation curves for a type-II superconductor in the absence of any pinning mechanism (M_{rev}, dashed) and in presence of bulk pinning only (drawn line) for increasing field ($M_\uparrow$) and decreasing field ($M_\downarrow$). H^* is the characteristic field above which vortices completely permeate the sample when the field is applied after zero-field cooling. Also shown are minor magnetisation loops ~~(dotted)~~ traversed when a field modulation or ac-field of moderate amplitude h_0 and frequency is superimposed on the dc-field. When the ac-field amplitude increases from $h_0 < H^*$ to $h_0 \gg H^*$ the minor hysteresis loops change shape from lenticular (minor loops (1) and (2)) to parallelogramatic (minor loop (4)). H_{irr} is the irreversibility field above which the effects of pinning can no longer be discerned. The little "humps" below H_{irr} illustrate the peak effect. The ratio between the upper and lower critical fields H_{c2} and H_{c1} corresponds to $\kappa \approx 2.5$.

induced bulk electrical shielding current $\mathbf{j}(\mathbf{r})$, obtained by combining Maxwell's equations with $E(j)$:

$$-\frac{\partial \mathbf{B}}{\partial t} = \nabla \times \mathbf{E}(j) \equiv \nabla \times \hat{\rho}(j) \nabla \times \mathbf{B} \tag{A3.2.1}$$

$$-\frac{\partial \mathbf{j}}{\partial t} = \nabla \times \nabla \times \mathbf{E}(j) \tag{A3.2.2}$$

In direct analogy with Ohmic conductors, magnetic flux entry and exit into the superconductor bulk is delayed with respect to the variation of the applied electromagnetic field, leading to flux density gradients and hysteresis of the local flux- and current destiny $\mathbf{j}(\mathbf{r})$ (here $\mathbf{r}$ is the position measured from the sample centre). When the field is increased, vortex lines enter at the sample edge so that the vortex density is highest there, and lowest in the sample center. When the magnetic field is decreased, vortices exit first through the sample boundary, while those in the center remain trapped, leading to magnetic remanence. Thus, the magnetic moment

$$m = \int_V |\mathbf{j}(\mathbf{r}) \times \mathbf{r}| \, d^3 r \qquad \text{(unit [Am}^2\text{])} \tag{A3.2.3}$$

is irreversible: the value of m depends on the path taken to reach the measurement field, as illustrated in figure A3.2.2 (V is the sample volume). The width of the main hysteresis loop is a direct measure of j_c, or, more generally, of the sustainable lossless current density, as will be discussed below.

A3.2.3.3 Self-organisation of the flux distribution and the flux front

The hysteresis is the result of vortex lines being (drastically) slowed down by repeated trapping by successive pinning centres as the screening current induced by the time-varying field pushes them into

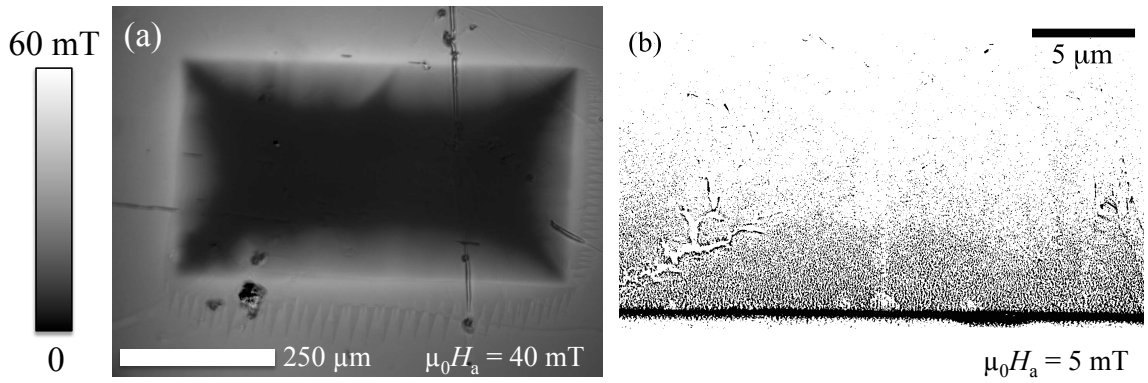

Figure A3.2.3: Imaging of initial vortex penetration into a $Ba(Fe_{0,93}Co_{0.07})_2As_2$ single crystal with strong pinning, at 10 K, after zero-field cooling. (a) a low-resolution magneto-optical image of the magnetic flux density shows the latter penetrates from the four edges of the rectangular sample, up to a well-defined flux front (bright areas correspond to high flux density B, black areas to $B = 0$). The inner region is in the Meissner state and therefore appears as black (spots are artefacts, and wedges are magnetic domains of the ferrimagnetic film used for imaging). (b) a Bitter decoration image reveals the individual vortices. After [Grisolia2013].

or out of the material. On first flux penetration (zero-field cooled condition), the nonlinear nature of the vortex-pin interaction leads to the presence of a well-defined flux front to which the first vortices have advanced. Behind the flux front, the vortices self-organise so as to maintain a flux density gradient $\nabla \times \mathbf{B}$ equal to the critical (or sustainable) current density. The local advances of the vortices into the superconductor are affected by the spatial variations of the "pinning landscape" and proceed in an avalanche–like manner. The flux front therefore has a rough profile, described by a nonlinear diffusion equation [Edwards and Wilkinson 1982]. At the characteristic field H^*, flux fronts entering from opposite sides of the sample merge, and the description in terms of self-organisation is no longer appropriate. The dynamics of vortices entering a type-II superconductor with pinning has been compared to that of a sandpile [de Gennes 1989].

A3.2.3.4 Modelling using a power-law $E(j)$–curve

The macroscopic hysteretic behaviour of (the local values of) $\mathbf{B}$ and $\mathbf{j}$ can be conveniently modelled by considering a model power law $E \propto (j/j_c)^n$ [Brandt 1996]. This corresponds to an empirical law sometimes used to characterise the quality of a wire, where a large value of n signifies a high material uniformity, and is also well-suited to quantitatively understand the effect of flux creep on magnetic hysteresis (see below). Note that $E \propto (j/j_c)^n$ smoothly interpolates between Ohm's law and the case of ideal flux pinning. In the first case, $n = 1$ and the material shows a linear electromagnetic response described by the skin effect; the effective depth to which the electromagnetic field penetrates the material is the skin depth $\delta = \sqrt{\rho/\mu_0\omega}$ where $\rho = \rho_n, \rho_f$ for a normal metal and a superconductor without pinning respectively, and ω is the angular frequency of the time-varying field. In the second case, $n \to \infty$; the response is very strongly nonlinear and adequately described by the Bean model.

A3.2.3.5 Bulk pinning and the Bean model

The Bean model [Bean 1962] consists of approximating the electromagnetic response of the superconductor by taking the working point on the materials' $E(j)$ (or IV) curve as fixed. In the case of near-perfect pinning without any measurable dissipation, i.e. $|\mathbf{v}| = |\mathbf{E}| = 0$ for $|\mathbf{j}| < j_c$, the working point is fixed at $|\mathbf{j}| = j_c$. As a consequence, the modulus $|\mathbf{j}| = \pm j_c$ throughout all regions of the material in which vortices

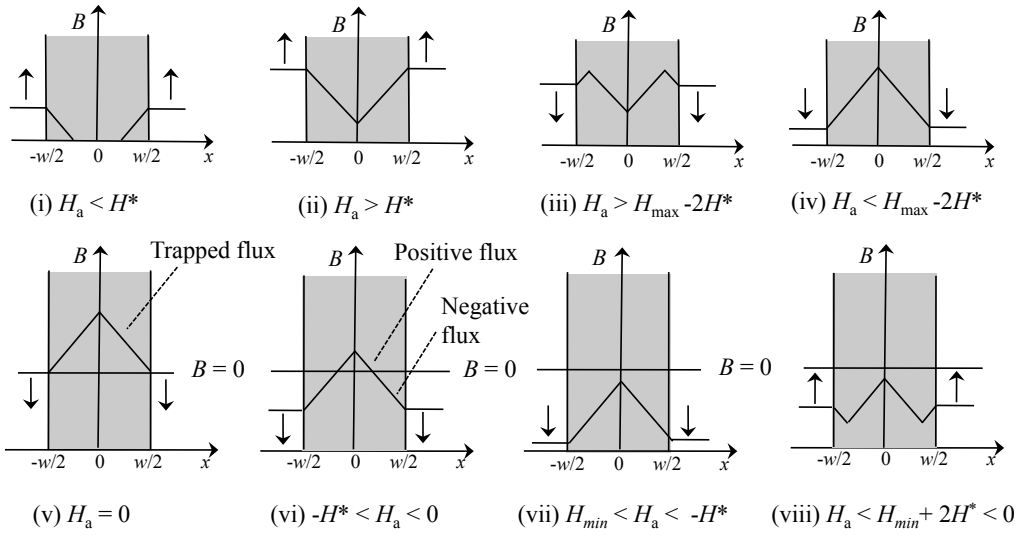

Figure A3.2.4: Distribution of the flux density B (or vortex density B/Φ_0) in a slab-shaped type-II superconducting sample occupying $|x| < w/2$, with the external magnetic field H_a applied along z, according to the Bean model, at various stages of the hysteresis loop (the y coordinate points into the plane). (i) $H_a < H^*$, the flux fronts penetrating from opposite edges have not yet met in the sample center ; (ii) Once $H_a > H^*$, $j = \pm j_c$ throughout the sample and the flux distribution does not change its shape; (iii) upon reduction of H_a from the maximum applied field H_{max}, the screening current density at the sample boundaries reverses sign and flux starts leaving the sample ; (iv) $H_a < H_{max} - 2H^*$: the direction of the flow of the screening (critical) current and therefore the shape of the flux density profile is now reversed throughout the sample; the flux profile does not change shape as H_a is reduced further; (v) when H_a is reduced to 0, trapped or "remnant" flux (vortices) remain in the sample; (vi) when H_a is reduced below 0, positive trapped flux co-exists with magnetic flux (vortices) of the opposite sign penetrating from the boundaries. If the Bean model does not imply any discontinuity of the screening current density at the interface between positive and negative flux, in real superconductors a vortex-free region appears because no vortices can exist when $H_a < H_{c1}$. In superconductors of thickness $2\lambda \ll d \ll w$, vortex lines wrap around this flux-free zone to form a so-called "current string" or "Meissner hole" [Indenbom 1995]. (vii) and (viii) the further decrease of H_a to a minimum (negative) value H_{min} and its subsequent increase entail flux distributions that mirror those in stages (ii) and (iii).

are present. That is, the magnetic flux density gradients obey

$$\left(\frac{\partial B}{\partial H_a}\right)^{-1}_{rev} |\nabla \times \mathbf{B}| = \left(\frac{\partial B}{\partial H_a}\right)^{-1}_{rev} \left|\left(\frac{\partial B_x}{\partial z}\right) - \left(\frac{\partial B_z}{\partial x}\right)\right| = j_c(\mathbf{B}), \tag{A3.2.4}$$

the "critical state equation". In all other regions of the material $\mathbf{B} = 0$ and $\mathbf{j}$ takes on the value required by the Biot-Savart law and the material geometry. In Eq. (A3.2.4), $\nabla \times \mathbf{B}$ has been written out to describe the flux gradients in an (xz)–planar section of a sample subjected to a magnetic field applied along the z-direction. One sees that for samples that are long in the direction of the applied magnetic field, the current density corresponds to a constant transverse flux gradient $-\partial B_z/\partial x$ (the flux density decreases as a straight line from the sample edge), while for a thin film in perpendicular field, it corresponds to the gradient $\partial B_x/\partial z$ of the parallel flux across the sample thickness.

For fields well above H_{c1} and for a Ginzburg – Landau parameter $\kappa = \lambda/\xi \gg 1$, the prefactor $(\partial B/\partial H_a)_{rev}$ (which follows from the slope of the reversible magnetisation curve) can be replaced by μ_0. One can then extract the modulus j_c of the current density from the integral in Eq. (A3.2.3), so that the difference between the (saturated) magnetic moments measured in increasing and decreasing

Geometry	$\Delta M_{sat} \equiv \Delta m_{sat}/V$ [A/m]	H^* [A/m]	I_c [A]	hysteretic losses	R_s
long thin sheet of thickness d and height $h \gg d$, $H \parallel$ to the surface	$j_c d/2$	$j_c d$	$j_c dh$	$\frac{4\mu_0\omega}{3\pi}\frac{h_0^3}{j_c d}$	$\frac{\sqrt{4\pi\mu_0}}{j_c}P_0^{1/2}$
thin strip of thickness d and width w, in perpendicular applied field	$j_c d/2$	$j_c d/\pi$	$2j_c dw$	$\frac{\pi^2\mu_0\omega}{12}\frac{h_0^4}{j_c^2 d^2}$	$\frac{4\pi}{j_c^2 d}P_0$
long thin cylinder or wire of radius R, $H \parallel$ to the surface	$2j_c R/3$	$j_c R$	$\pi j_c R^2$	$\frac{2\mu_0\omega}{3\pi}\frac{h_0^3}{j_c R}$	$\frac{\sqrt{4\pi\mu_0}}{j_c}P_0^{1/2}$
thin disk of thickness d and radius $R \gg d$ in perpendicular applied field	$2j_c R/3$	$j_c d/2$		$\frac{16\mu_0\omega}{3\pi^3}\frac{R}{d}\frac{h_0^4}{j_c^2 d^2}$	

Table A3.2.1: Bean model applied to various geometries : width $\Delta M_{sat} \equiv \Delta m_{sat}/V$ of the magnetisation loop at saturation ($H > H^*$, V is the sample volume); field of full flux penetration H^*; Critical current (for current applied along the longest direction of the sample) ; hysteretic losses per cycle (in the limit $h_0 \ll H^*$) when the sample is subjected to an ac field of angular frequency ω and amplitude h_0 [Clem and Sanchez 1994] ; Surface resistance R_s as function of incident microwave power density P_0 (electric field and current along the longest direction of the sample).

magnetic field $\Delta m_{sat} = |m_\uparrow - m_\downarrow| = \mathcal{C} j_c$, with $\mathcal{C}$ a constant that depends only on sample geometry. Hence, the Bean model can be applied to irreversible magnetisation curves to determine j_c from Δm_{sat}. It also follows that the reversible magnetisation lies midway between the increasing and decreasing field branches of the hysteresis loop (indicated in figure A3.2.2). Several important geometries relevant for experiments are summarised in Table A3.2.1.

A3.2.3.6 Bean–Livingstone barrier

The vortex ensemble in a type-II superconductor is stabilised by the inward force provided by diamagnetic screening currents circulating in the surface layer of thickness λ, which effectively forms a magnetic container. This force, which, by virtue of Eq. (A2.2.3), decays as $e^{-x/\lambda}$, with x the distance between a vortex line and an outer surface of the sample, counteracts the (outward) attractive force $\propto e^{-2x/\lambda}$ to the very same surface (see section *A3.2.2.2*). The superposition of the two forces results in an energy barrier acting against vortex entry into the sample as the applied magnetic field is increased.

As a result of this "Bean-Livingstone barrier", vortices are only admitted into the superconductor when the field reaches the first penetration field $H_p \simeq H_c > H_{c1}$. In the absence of bulk pinning, the surface screening current then pushes the vortices to the sample center. Contrary to the case of bulk pinning and the Bean model, the flux density on increasing the applied field is thus higher in the sample center that near its boundary. As more and more vortices accumulate in the sample, the screening current is increasingly compensated by the vortex currents, yielding a magnetisation that takes the general form $M_\uparrow \simeq -H_p^2/2H_a$ [Clem 1974]. Upon decreasing the magnetic field, vortex exit is counteracted by the surface screening current until the magnetic flux densities inside and outside the sample are equal, and the barrier disappears. Vortices can then exit freely, and the magnetisation $M_\downarrow \simeq H_{c1}/(\pi \ln\kappa) \approx 0$ [Clem 1974]. The resulting magnetic hysteresis loop, with near-zero magnetic moment for decreasing field as a hallmark, is shown in figure A3.2.5. The Bean-Livingstone barrier is significantly diminished in the presence of sharp corners on the sample, and can be quelled by appropriate surface treatment, yielding so-called "gates" for flux entry, ~~such as abrasion or irradiation,~~ or by treatment that smoothly diminishes T_c to zero at the surface, such as an oxygen diffusion layer at the surface of superconducting Nb or V.

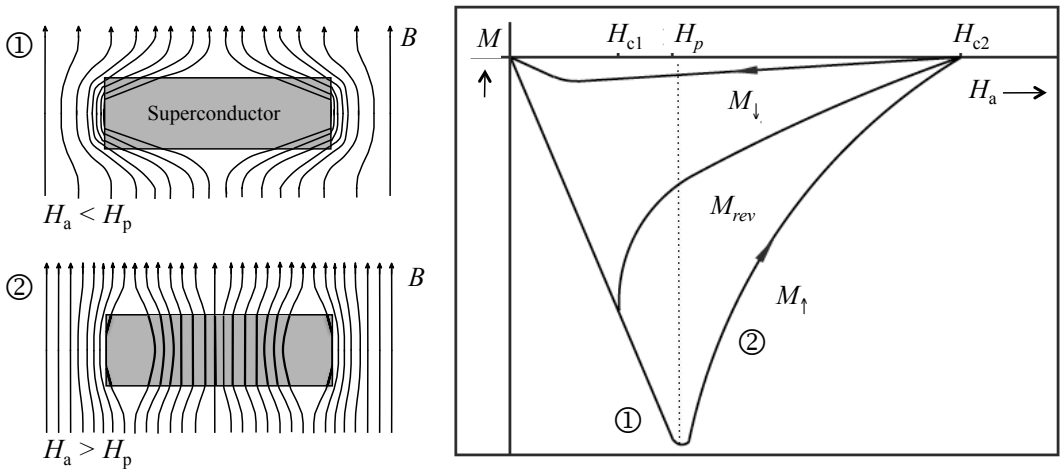

Figure A3.2.5: The effect of a Bean–Livingstone surface barrier on magnetisation in the absence of bulk pinning. Note the characteristics: the first penetration of flux occurs at $H_p \approx H_c$, the magnetisation is zero at $H_a = 0$, and the magnetisation for decreasing field $M_\downarrow$ is close to zero. The left-hand diagram (1) shows the situation for a platelet-like sample with a square cross-section at $H_a < H_p$, in which vortex line segments partially penetrate through the sharp corners (vertices) of the sample. Diagram (2) shows the situation for $H_a > H_p$: vortex lines accumulate in the center of the sample.

A3.2.3.7 Geometrical barrier

A second barrier effect appears in type-II superconducting samples of non-ellipsoidal cross-section; it concerns the vast majority of low-field transport and magnetisation experiments carried out on low-pinning materials, for these are typically carried out on rectangular strip- or platelet-shaped samples. Whereas the external field H_i at the surface (and therefore at the equator) of an ellipsoidal sample is enhanced according to the expression $H_i = H_a - n_x M_{rev}(H_i) \equiv \underline{H_a}$ (with the field H_a applied parallel to one of the principal axes (x) and n_x the corresponding demagnetisation coefficient), the magnetic field at the equator of non-ellipsoidal samples is effectively shielded by the screening currents circulating at the vertices (see Figure A3.2.5). Vortex line segments first (partially) penetrate through the sharp corners (vertices) of the sample. Full penetration only occurs when segments penetrating from the top and the bottom meet at the sample equator, whence they can enter freely. For strip- or bar shaped samples of thickness d smaller than the width w, the field of first penetration $H_p \simeq H_{c1}(2d/w)^{1/2}$ is larger than the penetration field $H_p^{ell} = H_{c1}(1 - n_x) \approx H_{c1}(2d/w)$ expected for an ellipsoidal sample of the same aspect ratio. The sample geometry, or shape, thus creates a geometrical barrier for increasing field [Zeldov *et al.* 1994]. For decreasing field, this barrier does not exist, leading to strong magnetic hysteresis at low fields $H_a \lesssim H_{c1}$. The shape of the hysteresis loop can be distinguished from that controlled by the Bean-Livingstone barrier through the behaviour of the magnetic moment in decreasing field. This approaches the reversible moment (section *A3.2.3.2*) and is therefore not zero.

Thus, the geometrical barrier dominates the low-field magnetic irreversibility and electrical transport properties of high-aspect ratio low-j_c strip-and platelet-shaped superconducting materials in perpendicular field. The geometrical barrier is suppressed by careful abrading of the sample to an ellipsoidal or pyramidal cross-section, or by the presence of burrs or sharp wedges on the sample surface (which act as vortex entry gates). Such treatment will reveal the bulk pinning properties. When the sample height in the field direction is larger than the width, flux penetration happens at H_{c1}, or is determined by the Bean-Livingstone barrier.

A3.2.3.8 Simultaneous presence of bulk pinning and a barrier

In type-II superconductors with intermediate j_c (so that the characteristic field $H^* \simeq H_{c1}$) both bulk pinning and the barrier will be manifest. Upon first flux penetration, the competition between surface screening currents and bulk pinning will lead to "flux puddles" : there is neither a well-defined front of penetrating vortices from the edges nor an accumulation of vortices in the sample center. Another effect of this intermediate situation is "edge contamination", whereby the vortex ensemble arrangement and the local critical current density are determined by disorder introduced at vortex entry because of local variations of the geometrical barrier or edge roughness [Paltiel *et al.* 2000].

A3.2.3.9 ac and High Frequency electromagnetic fields

The analysis of the ac response is a useful means to determine the critical current in conditions where dc magnetic measurements are insufficiently sensitive, but the critical current density is still too high to allow direct electrical transport measurements. The exposure of a type II superconductor to a time-varying (ac) magnetic field of amplitude h_0 superposed on the background dc field H_a results in a minor magnetisation loop being traversed, as indicated in figure A3.2.2 by M_{ac}. The sample response can be measured by various methods : the global complex ac susceptibility, $\chi \equiv (2\pi h_0)^{-1} \int M(H_a + h_0(t))\mathrm{e}^{-i\omega t} d\omega t$, the local complex "transmittivity", $T \equiv (2\pi\mu_0 h_0)^{-1} \int B(H_a + h_0(t))\mathrm{e}^{-i\omega t} d\omega t$, the response of a mechanical oscillator to which the sample is attached, or, at higher frequencies, through the frequency shift and phase shift of a resonant electromagnetic circuit or cavity containing the sample. In all cases the time-varying field results in a time-varying force on the vortex ensemble, which is made to oscillate in the pinning potential "landscape" in which it is embedded. The nature of the response depends on the magnitude of both h_0 and ω, and can be described by combining the (overdamped) vortex equation of motion

$$\gamma \dot{u} + f(u) = \mathbf{j} \times \mathbf{B} + \eta(t, T) \tag{A3.2.5}$$

with $\mathbf{E} = \mathbf{v} \times \mathbf{B}$ and Maxwell's equations. Here, $\gamma = B^2/\rho_f$ is the friction coefficient due to flux-flow losses, $\eta(t, T)$ is a stochastic noise term, and $\dot{u} \equiv v$.

The linear response regime of small h_0 is defined by the regime of vortex excursion u for which $f(u) \approx ku$, where the pinning restoring force constant k (unit [N/m^4]) is known as the Labusch constant. At frequencies $\omega > \omega_0 \equiv k/\gamma$, response is dominated by the friction force $\gamma\dot{u}$. Vortices perform periodic oscillations of amplitude much smaller than r_f. Therefore the details of pinning are irrelevant to the macroscopic ac response, which is entirely described by the flux-flow skin effect (with a skin-depth $\delta = \sqrt{\rho_f/\mu_0\omega}$). For $\omega < \omega_0$, the details of pinning come into play. For small h_0, the response is purely elastic; vortices perform reversible oscillations near their equilibrium pinned positions. The (lossless) macroscopic ac response in this so-called "Campbell regime" is in phase with the driving field and therefore "Meissner–like", but with a penetration depth $\lambda_C = \sqrt{B^2/\mu_0 k}$ determined by flux pinning [Campbell and Evetts 1972]. At very low frequencies $\omega \lesssim \omega_0 \mathrm{e}^{-U(j)/k_B T}$ the ac response is determined by thermally activated flux jumps (see below).

For larger $h_0 > F_p/\sqrt{\mu_0 k}$, the vortices can be depinned by the ac field. Depending on the strength of pinning, the low temperature electromagnetic response is determined by the Bean model, by the Bean-Livingstone barrier, or by the geometrical barrier. The response is hysteretic and strongly nonlinear; therefore, strong higher harmonic response appears. The nonlinearity can be detected most easily by measuring the third harmonic of the ac susceptibility. The conditions of temperature and magnetic field at which flux pinning becomes unobservable due to thermal activation define the so-called irreversibility line $T_{irr}(B, \omega)$ in the (T, B) (temperature-field) phase diagram. This can be readily determined from the (ω-dependent) demise of the third harmonic ac response. Note that the harmonic content of the ac susceptibility is very similar, irrespective of whether bulk pinning or a barrier is dominant. Only imaging measurements of the local flux density [Paltiel *et al.* 2000], or an in-depth analysis of the harmonic susceptibilities [van der Beek *et al.* 1996] can distinguish which situation is relevant.

Hysteretic losses and associated heating effects are very important because they determine the dissipation in superconducting transformers and motors, as well as the quality factor of radio-frequency (RF) and high-frequency (HF) superconducting devices such as detectors, resonators, and reception chains. The power loss-mechanism can be characterised through the measurement (at low frequency) of the ac losses or (at high frequency) of the surface resistance R_s as function of RF or HF power (see section A2.7.2). Some useful relations are summarised in Table A3.2.1.

A3.2.3.10 Measurement of the IV curve

In thin films, strips, or wires, or in low-j_c materials, the $E(j)$ curve can be directly assessed by the measurement of the current–voltage (IV) characteristic of the superconductor. It should be always borne in mind that the application of a (non-equilibrium) electrical transport current I to the superconductor in the mixed state gives rise to the same kind of irreversible properties as the application of a magnetic field. In the presence of bulk pinning, the Bean model applies [Zeldov *et al.* 1994]. As the magnitude of the electrical current is increased, this first flows along the sample edges, provoking vortex entry. As vortices move inwards, the current density is limited to $|\mathbf{j}| = j_c$ in the flux-penetrated regions; thus the total current grows through the increase of the width of the flux-penetrated regions rather than that of the local current density. The critical current I_c of the sample is reached when the flux fronts from opposite edges meet in the sample center. For $I > I_c$ and $H \gg H^*$, vortices transit freely through the sample. If $H \ll H^*$ and $I > I_c$, vortices carrying positive and negative flux enter from opposite edges and annihilate in the sample interior.

In the case of slab-shape samples (of thickness greater than 2λ) with weak bulk pinning, the Bean-Livingstone- and/or the geometrical barrier can sustain the flow of lossless current at the sample boundaries as long as the magnetic "self–field" produced by the current flow does not exceed the penetration field H_p. For currents larger than $I_c \sim H_p/d$, vortices of positive and negative flux enter from opposite sample boundaries and annihilate in the interior, leading to resistive losses.

It is important to note that while j_c is a property of the superconducting material, I_c is a property of the sample. Since non-uniformities give rise to rounding of the IV curve, it has been common practice to define j_c (rather arbitrarily) by a voltage criterion of 1 μV dropped over 1 cm.

A3.2.3.11 Thermal fluctuations and flux creep

Thermal fluctuations cause the vortex lattice to explore different metastable configurations in the pinning potential. In the absence of driving currents, this results in effectively larger pinning wells and an exponential reduction with increasing temperature of the pinning force, of the energy gain U_p due to pinning, and of the critical current density [Feigel'man and Vinokur 1990], well beyond the "trivial" temperature dependence entering via $H_c(T)$, $\xi(T)$ and $\lambda(T)$ (see Eqs. (A2.3.4) and (A2.3.5)).

In the presence of a driving force, vortices will be driven between metastable configurations of almost equal energy, a process that leads to a unidirectional creep of the vortex ensemble, accompanied by the reappearance of resistance for $|\mathbf{j}| < j_c$. The average velocity of the vortices is determined by the effective jump rate of the system between such states, which is a thermally activated process. The calculation of the average vortex velocity in the random pinning potential is a complicated problem of statistical physics; usually, the velocity is modelled using an activated law, such that

$$v = v_0 \mathrm{e}^{-U(j)/k_B T}, \tag{A3.2.6}$$

where $U(j)$ is the magnitude of the thermal activation barriers relevant for a driving current of density j, and v_0 is a prefactor related to the so-called "attempt rate". Formulated as such, the critical current density j_c corresponds to the driving force $\mathbf{j}_c \times \mathbf{B}$ at which all creep barriers vanish, i.e. $U(j_c) = 0$. For current densities smaller than but comparable to j_c, the average activation barrier is small and the vortex system can easily find new most favorable metastable states near to its actual one. The smaller

the current density, the lower the probability of a jump to an equivalent pinned configuration becomes, and the higher the average activation barrier $U(j)$. At low temperatures, the elastic properties of the vortex ensemble lead to nucleation-type creep and $U(j) \propto j^{-\mu}$ [Feigel'man *et al.* 1989], which diverges at low current densities (see subsection *A3.2.6.1* below). The current density-dependence of the average activation barrier gives rise to the highly nonlinear $E(j)$–curve of subsection *A3.2.3.1*,

$$E = \rho_0 \mathrm{e}^{-U(j)/k_B T}, \tag{A3.2.7}$$

which should be combined with Eq. A3.2.2 in order to describe the low-frequency electrodynamics of the superconductor. As far as the magnetic moment is concerned, the Bean model is usually still a good approximation, but j_c should be replaced by a time- or field sweep rate-dependent "sustainable current density" j_s as the new work point on the $E(j)$–curve. As a result, the width Δm_{sat} of the magnetic hysteresis loop is no longer indicative of the "true" critical current density but, rather, of the flux creep rate at different magnetic fields. An elementary rearrangement of terms shows that j_s satisfies

$$U(j_s) = k_B T \ln\left(\frac{t_i + t}{\tau}\right), \tag{A3.2.8}$$

where t is the time scale of the experiment, τ is a normalisation time, and t_i is the time on which transient effects are important. Information about the energy barrier $U(j)$ can be obtained by measuring the temporal relaxation, as a result of flux creep, of the saturated magnetic moment $m_{sat}(t)$ or the local induction $B(t)$ over the sample. From such measurements, the $U(j)$–curve can be directly obtained by plotting $k_B T \ln\left(c - |\partial m_{sat}/\partial t|\right)$ versus $\Delta m_{sat} \propto j_s$. Repeating the experiment at slightly different temperatures yields a series of curves over finite j intervals which can be overlapped so as to determine the constant c [van der Beek *et al.* 1992]. In this way the $U(j)$ dependence can be determined over several decades in j. In principle, this can also be achieved by waiting long enough ($\sim 10^{40}$ years) for the current to decay! The true j_c is obtained by extrapolating to $U = 0$. It is interesting to note that the $U(j)/k_B T$ ratio always falls within the range $10 - 30$. This remarkable observation can be understood in terms of the self-organising mechanism of creep and the experimental time window of the experiments.

The $U(j)$–curve can also be obtained from frequency-dependent measurements of the low-frequency ac response of the superconductor; then, the relevant barriers satisfy $U(j) = k_B T \ln(1/\omega\tau)$. Note that activation-type creep over the Bean-Livingstone barrier is also possible and leads to a time- or field sweep rate-dependent first penetration field $H_p(t)$. By contrast, the geometrical barrier is proportional the product of the vortex line energy $\varepsilon_0 = 4\pi\xi^2\left(\frac{1}{2}\mu_0 H_c^2\right)$ (with unit [Jm^{-1}]) and the sample thickness. It is therefore of macroscopic nature, and cannot be overcome by thermally activated vortex motion.

A3.2.3.12 Pinning energies and activation barrier

In very many reports in literature, the flux creep activation barrier $U(j)$, which is related to non-equilibrium dynamics and transport properties, is confused with the pinning energy U_p, which corresponds to the free energy gain of the pinned vortex system with respect to the hypothetical unpinned vortex lattice in the same material. It is important to stress that these quantities are not trivially related. Notably, U_p cannot be extracted from electrical or inductive transport measurements, while $U(j)$ can.

A3.2.4 Statistics of Pinning : From the elementary force to the critical current density

Vortex lines are made of only magnetic flux and electrical current. They are therefore flexible objects – in fact, the softest "matter" in nature – that can be characterised by a set of elastic constants. These are the (single) vortex line tension $\varepsilon_l \approx \varepsilon^2 \varepsilon_0$, and the vortex lattice compression, tilt, and shear moduli $c_{11}(\mathbf{k})$, $c_{44}(\mathbf{k})$, and c_{66}. The compression- and tilt moduli are dispersive and depend on the wave vector $\mathbf{k} = (k_{xy}, k_{\|})$ of the elastic distortion. For many estimates in the intermediate field regime $B_{c1} \ll$

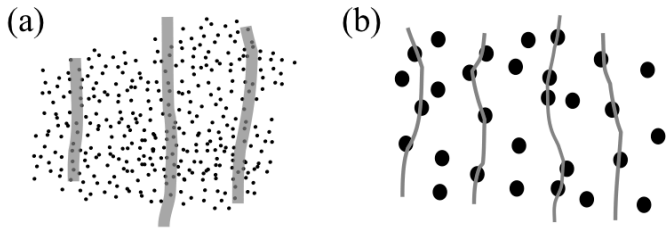

Figure A3.2.6: Cartoon of weakly (a) versus strongly pinned vortex lines (b). Black dots depict pinning centres and grey lines represent the vortex cores.

$B \lesssim 0.2B_{c2}$, the approximations $c_{44}(\mathbf{k}) \sim \varepsilon^2\varepsilon_0 a_0^{-2}(1-b)$ and $c_{66} \approx (\varepsilon_0/4a_0^2)(1-b)^2(1-0.29b)$ are useful. Here $\varepsilon \equiv \xi_c/\xi_{ab}$ is the anisotropy parameter for uniaxially anisotropic superconductors, and $b \equiv B/B_{c2}$. In anisotropic and layered superconductors, ε, and, by consequence, the vortex tilt modulus is small. Vortices can therefore easily bend to better adapt to the pinning landscape.

In the absence of bulk flux pinning, vortex lines form the regular Abrikosov lattice. In the presence of pinning, the vortex ensemble distorts as a result of the forces f_p exerted by each inhomogeneity or defect. The vortex displacement field $\mathbf{u}(\mathbf{r})$ mirrors the local equilibrium between the pinning forces and the elastic restoring force of the vortex ensemble, and corresponds to a given metastable configuration, and therefore to a local energy minimum in "vortex configuration space". The free energy gain (per unit volume) with respect to the unpinned Abrikosov lattice is the pinning energy U_p. The volume pinning force F_p is the force needed to drive the vortex ensemble to another energy minimum.

An essential ingredient of any calculation of F_p is the determination of the volume of vortex ensemble involved in a particular change of configuration, i.e., the volume of the vortex ensemble that can be considered as "pinned independently". When the pinning forces f_p are very weak, the vortex lattice is only very slightly perturbed. Any change of configuration will entail slight readjustments of vortex lines over a large "correlation volume" $V_c = R_c^2 L_c$. Here R_c and L_c are correlation lengths transverse and parallel to the field direction. The larger the pinning forces are, the smaller V_c, since a local adjustment will be insufficient to entail rearrangements of well-pinned far-away vortices.

A3.2.4.1 Point defects : Weak collective pinning

"Weak" or "collective" pinning corresponds to the situation of a large density $n_d \gg r_f^{-2}L_c^{-1}$ of randomly distributed weak and small pinning centres (i.e. of dimensions $\ll r_f$) [Blatter *et al.* 1994, Blatter, Geshkenbein, and Koopman 2004]. Such defects typically correspond to vacancies, interstitials, dopant atoms, small voids, small dislocation loops, or other atomic-sized impurities. The seminal collective pinning theory of Larkin and Ovchinnikov [Larkin and Ovchinnikov 1979] introduces the correlated volume as that over which the average relative vortex displacement $\langle|\mathbf{u}(\mathbf{r})-\mathbf{u}(0)|^2\rangle^{1/2}$ induced by pinning remains smaller than r_f. The forces exerted by all pinning centres in the volume V_c compete, so that the average (i.e. the first moment of the) total force F_c vanishes. Hence, the vortex ensemble is only pinned by the fluctuations of F_c. The largest non-zero moment $\delta F_c = (n_d V_c \langle f^2\rangle)^{1/2}$, where $\langle f^2\rangle \approx \frac{1}{2}f_p^2$ is the mean square of $f(r)$ averaged over a primitive cell of the vortex lattice with area Φ_0/B. A pinning strength, or mean-squared pinning force density, can be defined by $W \equiv n_d\langle f^2\rangle \approx \frac{1}{2}n_p f_p^2$ in order to express the volume pinning force as

$$F_p = \delta F_c/V_c = (W/V_c)^{1/2}. \tag{A3.2.9}$$

Note that W is related to the strength of the short range correlations $\langle U_{pin}(\mathbf{r})U_{pin}(\mathbf{r}')\rangle = \gamma_U\delta(\mathbf{r}-\mathbf{r}')$ of the local energy gain $U_{pin}(\mathbf{r})$ introduced in Ref. [Blatter *et al.* 1994] as $W = \gamma_U/a_0^2$. The notation of

Ref. [Blatter *et al.* 1994] is meaningful for fields $B < 0.2B_{c2}$ and expresses the fact that only the vortex core area is involved in pinning.
To proceed further, one has to compute V_c from the balance between the energy loss due to tilt- and shear deformations (see section A4.2.4), on the one hand, and the work done by the pinning centres on the other hand :

$$\frac{1}{2}c_{44}\left(k_{xy} \approx \frac{\pi}{R_c}\right)\left(\frac{r_f}{L_c^2}\right) = \frac{1}{2}c_{66}\left(\frac{r_f}{R_c^2}\right) = \left(\frac{W}{R_c^2 L_c}\right)^{\frac{1}{2}} r_f. \qquad \text{(A3.2.10)}$$

It should be noted that the dispersion of the tilt modulus c_{44} plays an important role. This leads to

$$L_c = [c_{44}(0)/c_{66}]^{\frac{1}{2}} R_c; \qquad \lambda_h \ll R_c \ll L_c \qquad \text{(A3.2.11)}$$

$$L_c = [c_{44}(0)/c_{66}]^{\frac{1}{2}} R_c^2/\pi\lambda_h; \qquad R_c \ll L_c \ll \lambda_h \qquad \text{(A3.2.12)}$$

for local and non-local elasticity respectively. Here $\lambda_h = \lambda/(1-b)^{1/2}$. The limit of so-called "single vortex pinning" is reached when the pin energy gain (the right-hand member of equation (A3.2.10)) becomes too large to be accommodated by shear distortions. This can be expressed by putting $R_c = a_0$. The independently pinned objects are now single flux line segments of length

$$L_c \simeq \left(\frac{c_{44}(0)a_0^3 r_f}{\lambda_h^2 W^{\frac{1}{2}}}\right)^{\frac{2}{3}} \approx \varepsilon r_f \left(\frac{j_0}{j_c}\right)^{1/2}. \qquad \text{(A3.2.13)}$$

The second equality allows one to rapidly estimate the pinning regime that one is dealing with from the measured value of j_c. In practice, single vortex pinning occurs quite frequently, notably in cuprate– and iron-based high temperature superconductors, in the intermediate field regime above 1-2 T, but below $0.2B_{c2}$ [van der Beek *et al.* 2010]; in this field regime, it give rise to a field–independent

$$j_c \approx j_0 \left(\frac{27 n_d \langle f_p^2 \rangle r_f^3}{16\varepsilon\varepsilon_0}\right)^{2/3}. \qquad \text{(A3.2.14)}$$

At higher fields, relevant for disordered superconducting films and alloys, single-vortex pinning results in dome-shaped F_p versus B curves, well-described by a scaling relation $F_p \propto B_{c2}^n(T) b^p (1-b)$ with $n \approx 2.5$ and $p = \frac{7}{6}$ for δT_c pinning and $p = \frac{15}{6}$ for $\delta\ell$ pinning [Kes 1992].

In cuprate- and iron-based high temperature superconductors, the magnitude of the single vortex critical current density is typically some 10^4–10^5 Acm^{-2} at 4 K. In the $Bi_2Sr_2Ca_yCu_{1+y}O_{6+2y}$ family of layered cuprate superconductors, some organic superconductors, or in artificial superconductor multilayers, $\varepsilon \ll 1$ and the longitudinal correlation length L_c can be smaller than the spacing s between superconducting layers. So-called "pancake vortices" corresponding to the intersection of the vortex lines with individual superconducting layers are then pinned (and depinned) independently. The critical current density in this "single pancake" regime may exceed 10^6 Acm^{-2}. For example, pancake vortices are individually pinned by oxygen vacancies in $Bi_2Sr_2CaCu_2O_{8+\delta}$ [Li *et al.* 1996], a mechanism that accounts for j_c values at low temperatures as large as $0.1j_0 \approx 4 \times 10^{10}$ Am^{-2}. However, these current densities are not accessible because the correspondingly small small pinning creep barriers result in very strong flux creep effects as well as a low-lying irreversibility line.

In weakly pinning superconductors such as MgB_2, dichalcogenides, or amorphous metallic thin films, L_c can, on the contrary, be very large and the three-dimensional collective pinning (3DCP) scenario described by equation (A3.2.10) is realised. Critical current densities are then, typically, of the order $j_c \lesssim 10^2 - 10^3$ Acm^{-2}.

In thin films the situation where $L_c \gg d$ can arise when the magnetic field is perpendicular to the film. Vortex line cores then remain undistorted across the film thickness d, and disorder of the vortex ensemble

only develops because of shear deformations. As regards flux pinning, the materials then behaves two-dimensionally. In this limit of two-dimensional collective pinning (2DCP), R_c follows by substituting $L_c = d$ in equation (A3.2.10) giving

$$R_c \approx 2r_f c_{66} \left[2\pi d/W \ln(w/R_c)\right]^{1/2}. \tag{A3.2.15}$$

Here w is, again, the width of the film. Good agreement is obtained [Kes 1992, Wördenweber and Kes 1986] between this expression and experiment. The "single pancake" regime in layered superconductors can be considered a peculiar realisation of 2DCP.

A3.2.4.2 Point defects: Strong pinning

The limit of so-called strong pinning [Ovchinnikov and Ivlev 1991] corresponds to sparse ($n_d \ll r_f^{-2} L_c^{-1}$) randomly distributed large, strong pinning centres. It concerns the vast majority of type-II superconductors, and nearly all technological superconductors, in which strong pinning centres are responsible to critical current density values above 10^6 or even 10^7 Acm^{-2}. Strong pinning centres are typically nm-sized second phase inclusions, voids, or nm-scale modulations of the superconducting properties; their (maximum) pinning force f_p usually results from the combined effect of core– and electromagnetic pinning. In such situations, the net pinning force F_c over a correlated volume does not average out. Therefore, the volume pinning force $F_p = (a_0^2 d)^{-1} \Sigma_i^N f_p^i = f_p / a_0^2 \overline{\mathcal{L}}$ is the direct sum of the pinning force exerted by each defect the vortex line encounters over the sample thickness d. Any vortex line will be pinned on average by $N = d/\overline{\mathcal{L}}$ defects, where $\overline{\mathcal{L}}$ is the average distance between "effective" pinning centres that the line can reach. N is again limited by the elastic properties of the vortex ensemble. For low fields, vortex line excursions are limited by the line tension ε_l, and [Demirdis *et al.* 2013, Blatter, Geshkenbein, and Koopman 2004, van der Beek *et al.* 2002]

$$j_c(0) = \frac{f_p}{\Phi_0 \overline{\mathcal{L}}} = \pi^{1/2} \frac{f_p}{\Phi_0 \varepsilon} \left(\frac{f_p n_d r_f}{\varepsilon_0} \right)^{1/2} \qquad (B \ll \tilde{B}). \tag{A3.2.16}$$

Above the crossover field $\tilde{B} = \Phi_0 \left(\varepsilon \varepsilon_0 r_f / f_p\right)^2$, the repulsion between vortices is limiting, and the critical current density follows the behaviour expected for three-dimensional strong pinning [Demirdis *et al.* 2013, Blatter, Geshkenbein, and Koopman 2004, van der Beek *et al.* 2002],

$$j_c(B) = \frac{f_p}{\Phi_0 \overline{\mathcal{L}}^2} \frac{\varepsilon a_0}{\pi} = \frac{f_p}{\Phi_0 \varepsilon} \left(\frac{f_p n_d r_f}{\varepsilon_0} \right) \left(\frac{\Phi_0}{B} \right)^{1/2} \qquad (B \gg \tilde{B}), \tag{A3.2.17}$$

i.e. $j_c \propto B^{-\alpha}$ with $\alpha = \frac{1}{2}$. Such behaviour is ubiquitous in high-temperature superconducting thin films and composite conductors [van der Beek *et al.* 2002, Mele *et al.* 2019]. The set of equations (A3.2.16) and (A3.2.17) can be combined to obtain an experimental estimate of $f_p = (\Phi_0 \varepsilon / \pi) \left\{ j_c^2(0) / \left[\partial j_c(B) / \partial B^{-1/2} \right] \right\}$ from the low-temperature, low-field current density $j_c(0)$ and the slope $\partial j_c(B) / \partial B^{-1/2}$ at intermediate fields.

A crossover from weak collective to strong pinning can occur through various scenarios. In the presence of both strong and weak pins, the former will determine the critical current density at low fields. When all strong pins are occupied by vortices, the weak background pinning will take over and determine j_c. If pinning is determined by a single type of point defect, long-range fluctuations (on length scales $\gg r_f$) of the average defect density can give rise to strong pinning, while short-range randomness is responsible for weak collective pinning [Demirdis *et al.* 2013]. Finally, the presence of weak pins can slow down thermally activated vortex motion between strong pins (see, *e.g.*, [Sadovskyy *et al.* 2015]).

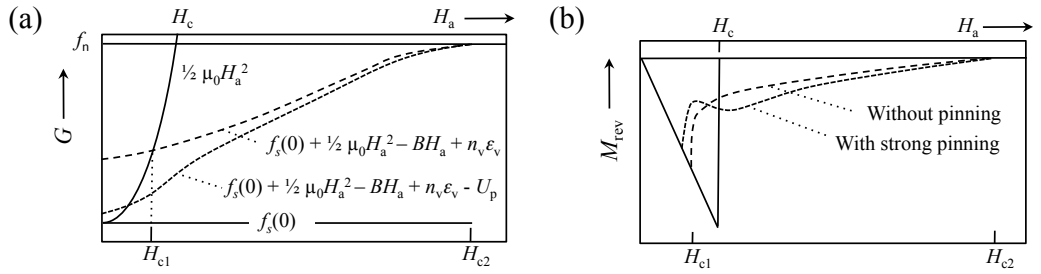

Figure A3.2.7: Schematic evolution of (a) the free energy G and (b) the reversible magnetisation $M_{rev} = -\partial G/\partial \mu_0 H_a$ for a type I superconductor (drawn line), a type II superconductor without pinning (dashed lines) and a type-II superconductor with strong pinning centres (dotted lines). In the latter case, the free energy paid per vortex is less than in the absence of pinning. The s-shape of $M_{rev}(H_a)$ is due to all pinning centres becoming occupied at intermediate field strengths.

A3.2.4.3 Pinning by correlated disorder

A particular form of strong pinning concerns extended correlated defects. These comprise "one dimensional" pins in the form of edge- and screw dislocation cores such as are commonly found in high-temperature superconducting films showing Vollmer-Weber (island) or Stransky-Krastanov (island plus layer) type growth, and purposely included linear defects such as columnar second phase inclusions ("nanorods") [Mele *et al.* 2019] and heavy-ion irradiation induced amorphous latent tracks [Bourgault *et al.* 1989, Civale *et al.* 1991, Nelson and Vinokur 1992]. Two-dimensional pinning defects include platelet-like inclusions, grain boundaries, anti-phase boundaries, twin boundaries in superconductors with an orthorhombic crystal structure, as well as the intrinsic structure of layered superconductors in a magnetic field applied parallel to the layers [Kwok *et al.* 1991]. Because of their ability to trap vortex lines along their entire length, such defects give rise to a profound anisotropy of pinning-related quantities, distinct from any anisotropy related to the crystal structure or electronic properties of the host material (see *e.g.* [Bartolomé *et al.* 2019]). The defect-induced anisotropy manifests itself through a cusp-like behaviour of the critical current density and the flux creep activation barriers for field aligned with the defect direction.

A3.2.5 Thermodynamics of the mixed state

In addition to the work associated with Meissner expulsion $\frac{1}{2}\mu_0 H_a^2$ and the energy loss $n_v\varepsilon_v$ associated with admitting vortex lines [Brandt 2003], the Gibbs free energy (per unit volume) of the mixed state (with respect to the normal state)

$$G = f_s(T) - f_n(T) + \frac{1}{2}\mu_0 H_a^2 - BH_a + n_v\varepsilon_v - U_p - k_B TS \tag{A3.2.18}$$

also includes the contribution U_p from flux pinning and the entropy contribution. The latter is the sum of the configurational entropy due to positional disorder of the vortices and the contribution from vortex thermal fluctuations. Both pinning and entropy lower the energy per vortex and, therefore, the free energy of the mixed state. As a consequence, flux pinning lowers H_{c1}, and increases H_{c2}. It also modifies the specific heat $c_p = -T(\partial S/\partial T)_p$ [van der Beek *et al.* 2005] and the reversible magnetisation

$$M_{rev} \equiv -\frac{1}{\mu_0}\left.\frac{\partial G}{\partial H_a}\right)_T = -\frac{1}{\Phi_0}\frac{\partial G}{\partial n_v}\left(\frac{\partial B}{\partial H_a}\right) \equiv -\frac{\mu_v}{\Phi_0}\left(\frac{\partial B}{\partial H_a}\right) \tag{A3.2.19}$$

which plays the role of the vortex chemical potential μ_v. In the presence of pinning, the equilibrium density of vortices in the superconductor is higher, and $|M_{rev}|$ lower than when pinning is absent. Therefore, a careful measurement of the reversible magnetisation yields direct information on the pinning energy U_p.

While this task is usually difficult due the hysteresis described in subsection *A3.2.3.2*, it can be used in the magnetically reversible vortex liquid state (see below), as well as through vortex imaging in materials with large local modulations of the pinning energy [Demirdis *et al.* 2010]. The effect of pinning on thermodynamic properties is large in superconductors with very strong pinning, e.g. that induced by amorphous columnar defects introduced by heavy–ion irradiation. An example is the reversible magnetisation curve of heavy–ion irradiated single crystalline $Bi_2Sr_2CaCu_2O_{8+\delta}$, which has an s-shape due to the fact that at small fields $B \ll B_\phi \equiv \Phi_0 n_d$ vortices can profit from the pinning energy, whereas this is prohibited for $B \gg B_\phi$ because all columnar defects are occupied [van der Beek *et al.* 1996] (see Figure A3.2.7). From such measurements, the pinning energy and the configurational entropy of the vortex ensemble can be obtained. Similar results where obtained on heavy–ion irradiated single crystalline $YBa_2Cu_3O_{7-\delta}$ and (Ba,K)BiO_3 [van der Beek *et al.* 2005].

A3.2.6 Vortex states and phase transitions

In a "clean" type–II superconductor without any flux pinning, inter–vortex repulsion leads to an arrangement into the triangular Abrikosov lattice. While details of the superconductors' electronic structure may modify the structure and even the symmetry of the Abrikosov lattice, the change of the free energy of the mixed state due to pinning as well as to the entropy related to thermal fluctuations induce a more profound change into disordered states of "vortex matter".

As all elastic objects in spatial dimension $d < 4$, the vortex ensemble in type-II superconductors is inherently unstable to the presence of a random disorder potential [Larkin and Ovchinnikov 1979, Imry and Ma 1975]. Therefore, any amount of pinning, however small, will disrupt the long-range positional and orientational order of the Abrikosov lattice. For very weak pinning, the length scale on which longe range order is undone can be excessively large and entail thousands of lattice parameters a_0 [Kim *et al.* 1998]. In the opposite limit of very strong pinning, the vortex ensemble is entirely amorphous; it is even possible to observe local density fluctuations of the vortex ensemble due to pinning [Demirdis *et al.* 2010]. However, it is not the breaking of long-range positional and orientational order, but the breaking of gauge symmetry that properly classifies vortex states.

A3.2.6.1 The vortex glass

In the (low-temperature) vortex glass state [Fisher, Fisher, and Huse 1991], all vortices are localised in a pinning-induced metastable state. Even if local thermal fluctuations are present [Feigel'man and Vinokur 1990], no thermally activated jumps are possible in the absence of a driving force. Thus, the global configuration of the phase of the superconducting order parameter is fixed; there is long-range phase order, and gauge symmetry is broken with respect to the normal metallic state. The localisation of vortices implies the divergence of creep barriers for vanishing driving force, i.e. $U(j) \to \infty$ for $j \to 0$ and a truly zero resistivity $\rho \sim \rho_f \mathrm{e}^{-U(j)/k_B T}$. In practice, this is achieved because of the elastic nature of the vortex ensemble. As the driving force decreases, only vanishingly rare and large activation nucleii – large vortex "bundles" in the language of the collective creep theory [Feigel'man *et al.* 1989, Blatter *et al.* 1994] or very large scale vortex re-arrangements in the language of the vortex glass theory [Fisher, Fisher, and Huse 1991] – can be made to expand and bring the vortex ensemble to another metastable state. For vanishing driving force, no activation nuclei can expand sufficiently, whatever their size, and the vortex ensemble always falls back into its original configuration. As a result, the energy barriers for creep grow according to $U(j) \sim U_c\,(j_c/j)^\mu$. The exponent μ depends on the dimensionality of the elastic medium and of the environment, and ranges from $\frac{1}{7}$ for single vortex lines to $\frac{16}{9}$ for large "bundles". When the vortex glass is subjected to an ac driving force, periodic

jumps between pairs of metastable states are allowed since these do not break long–range phase order [Koshelev and Vinokur 1990].

A3.2.6.2 The Bragg glass

In the case of weak collective pinning, the average relative vortex displacements characterised by the correlation function $B(r) \equiv \langle |\mathbf{u}(\mathbf{r}) - \mathbf{u}(0)|^2 \rangle$ are small, and grow with of vortex separation r as [Giamarchi and Le Doussal 1994, Giamarchi and Le Doussal 1995]

$B(r) \propto r \quad (r < R_c)$ - the so-called collective pinning or "Larkin" regime
$B(r) \propto r^{2\zeta} \quad (r < R_a)$ - the random manifold regime, with the wandering exponent $\zeta \sim 0,44$
$B(r) \propto \ln r \quad (r > R_a)$ - the charge density wave regime.

R_a is the distance at which relative displacements are larger than the vortex spacing and dislocations appear. For very weak pinning R_a may be larger than the sample size [Kim *et al.* 1998]. One then speaks of a "Bragg glass", since the vortex glass will show the usual Bragg diffraction pattern of the Abrikosov lattice, albeit with power-law rather than exponential tails of the diffraction peaks [Giamarchi and Le Doussal 1994].

A3.2.6.3 The Bose glass

In the case of correlated disorder, both the pinning energy and the dynamics of the vortex ensemble are strongly anisotropic. In particular, the anisotropy of the pinning energy leads to an anisotropic phase boundary of the vortex glass, with a higher transition temperature to the vortex liquid (see below) when the field is aligned with the defect direction. Flux creep is also highly anisotropic. For fields aligned with the defects, creep is of nucleation type [Nelson and Vinokur 1992]. For misaligned fields vortex motion proceeds by sliding of vortex "kinks" between defects [Schuster *et al.* 1994], which is only hindered by background pinning by point-like defects. Thus, the values of the creep exponent μ are strongly dependent on the field orientation angle. This type of anisotropic vortex glass has been termed "Bose-glass", due to the analogy between the system of vortex lines interacting with parallel correlated defects and the world lines of interacting bosons in two dimensions in a random potential.

A3.2.6.4 The vortex liquid

The vortex liquid state [Brézin, Nelson, and Thiaville 1985] occupies the high-temperature high–field region of the mixed state, and therefore separates the vortex glass from the normal state. The vortex liquid state is characterised by diffusive vortex motion : the vortex ensemble can access (many different) metastable configurations even in the absence of a driving force. As a result, the phase and amplitude of the superconducting order parameter at every position fluctuate in time. The linear resistivity is non-zero even in the limit of small currents, $j \to 0$. Therefore, the vortex liquid state does not break gauge symmetry and has electrodynamic properties that are formally equivalent to the normal state, even if the Cooper pair density is clearly non-zero on average, supercurrents and vortices can still be defined, and vortices can still be pinned [van der Beek *et al.* 1996] – although only on a finite time scale.

If defects are absent or the effect of thermal fluctuations [Feigel'man and Vinokur 1990] is very pronounced, pinning is very weak and vortex motion in the liquid state gives rise to the usual flux resistivity ρ_f. However, the presence of pinning in the liquid state may considerably slow down vortex motion. The resistivity

$$\rho_{TAFF} \approx \rho_f \mathrm{e}^{-U_c/k_B T} \tag{A3.2.20}$$

is then determined by thermally assisted flux flow, or TAFF [Kes *et al.* 1989]. The energy barrier U_c is related to the plastic deformations of the vortex ensemble; it provides a current-independent upper bound (cut-off) for the diverging glassy barriers at low driving force, thus enabling flux flow. Whereas

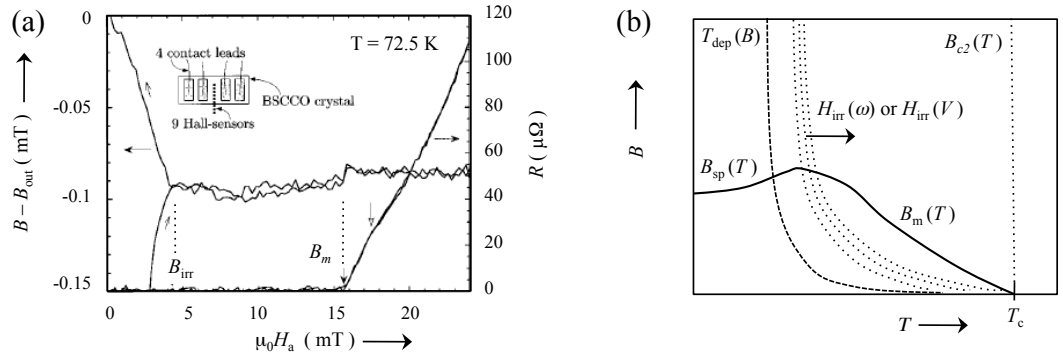

Figure A3.2.8: (a) Typical curves of the local magnetisation (defined as the difference between the local flux density B and the applied field $B_{\rm out} = \mu_0 H_a$) and the resistivity of $Bi_2Sr_2CaCu_2O_{8+\delta}$ single crystal. The curves show the first order from the Bragg glass to the vortex liquid phase at the ("melting") field B_m as a simultaneous discontinuity in both physical quantities. Flux pinning in the sample bulk can no longer be discerned above the irreversibility field B_{irr}. After [Fuchs *et al.* 1998]. (b) Schematic vortex matter (B,T) phase diagram in a generic clean type-II superconductor. The "melting" field B_m constitutes a first order phase transition from the vortex solid to the vortex liquid state. It is prolonged into the low-temperature regime in which flux pinning manifests itself as the so-called "second peak transition" at B_{sp}, which also overlies a first order phase transition. The depinning temperature T_{dep} marks the onset of an exponential decrease of j_c with temperature, and the demise of pinning. Also marked are various irreversibility lines $B_{irr}(T,\omega)$ above which pinning in the bulk becomes indiscernible, depending on the measuring frequency ω or the voltage threshold criterion / working point V.

in very thin ($d \ll L_c$) films U_c is the activation barrier for the motion of unbound dislocations or disclinations in the vortex lattice [Nelson and Halperin 1979], it is generally admitted that in disordered three-dimensional superconductors vortex diffusion is made possible through the mechanism of vortex cutting and reconnection. This process is very much facilitated in layered superconductors, comprising certain organic materials and the high-temperature cuprates and iron-based superconductors. Namely, the layeredness of these materials leads to a strong reduction of the vortex line tension and the vortex lattice tilt modulus, which promotes vortex line wandering and bending, processes that in turn lower the activation barrier for flux cutting. In extremely anisotropic materials such as $Bi_2Sr_2CaCu_2O_{8+\delta}$, the cutting and reconnection process can take place on the scale of a single layer, involving the exchange of single "pancake vortices" between vortex lines.

A3.2.6.5 Depinning transitions

When the thermal vortex displacements [Feigel'man and Vinokur 1990] exceed the range of the elementary pinning force r_f the pinning energy and the critical current density will decrease exponentially by thermal smearing. This rapid "softening" of pinning, marked by a sudden decrease of the irreversibility [van der Beek *et al.* 1996, Thompson *et al.* 1997, Fuchs *et al.* 1998], can be described by a "depinning line" or "depinning temperature" T_{dep} in the (T,B) phase diagram [Feigel'man and Vinokur 1990]. By comparing length scales it is clear that at low fields (i.e. $B < 0.2B_{c2}$) the depinning line, which as such does not constitute a phase transition, should lie below the melting line (see below), whereas the opposite is true at high fields. The "depinning line" is to be distinguished from the "irreversibility line" of section *A3.2.3.9* – the first is associated with the intrinsic temperature dependence of pinning properties, while the second denotes the temperature at which pinning becomes unobservable using a given experimental technique.

A3.2.6.6 The Bragg glass to vortex liquid transition

In superconductors with very weak bulk pinning, the vortex Bragg glass phase transforms to the vortex liquid through a first-order transition, often denoted "vortex lattice melting" [Brézin, Nelson, and Thiaville 1985, Brandt 1989, Zeldov *et al.* 1995]. The transition to the liquid state is driven by the excess entropy of the latter; as a result, the liquid has a higher vortex density than the Bragg glass. On the contrary, upon cooling the Bragg glass is stabilised through the gain in elastic deformation energy associated with the arrangement of vortices into a regular array. The first order melting transition is hysteretic, with the vortex liquid showing supercooling. The transition is enabled by thermal fluctuations of vortex segments (or kinks) around their equilibrium positions, until at the transition, plastic barriers of height U_c can be overcome [Fendrich *et al.* 1995, López *et al.* 1997]. At that point, thermal cutting and reconnection leads to the demise of the "identity" of vortices, and to entanglement in the vortex liquid state [López 1996]. The first-order transition has often been described by a Lindemann criterion: the vortex lattice "melts" when the thermal displacements become larger than a fraction $c_L a_0$ of the inter-vortex spacing [Brandt 1989]. Here c_L is the Lindemann constant, $c_L \approx 0.2$. This criterion, which is tantamount to a modified Ginzburg criterion for superconducting fluctuations, gives rise to a transition line in the (T, B) phase diagram which, for conventional superconductors, is located near the upper critical field $H_{c2}(T)$. For layered superconductors such as $Bi_2Sr_2CaCu_2O_{8+\delta}$, the transition lies at fields below 1 T.

The "vortex lattice melting" transition is characterised by latent heat [Schilling *et al.* 1996], by a discontinuous jump in the local induction (vortex density) [Zeldov *et al.* 1995], and by a sharp jump in the resistivity [Safar *et al.* 1992, Kwok *et al.* 1992]. Since the transition occurs at a temperature higher than the depinning transition of the Bragg glass [Fuchs *et al.* 1998], the jump of the resistivity at the transition is to be associated with the demise of the Bean–Livingstone and / or the geometrical barrier due to the collapse of the vortex line tension. The term "vortex lattice melting" is very often misused, through the association with other experimental observations. It should be reserved for the case described here, i.e. a thermodynamic temperature-driven first-order transition from the vortex lattice- or Bragg glass to the vortex liquid state.

A3.2.6.7 The vortex-glass to vortex liquid transition

In superconductors with strong pinning, as well as at high magnetic fields where the depinning temperature lies above the first order melting line, the disordered vortex glass phase transits continuously to the vortex liquid. Since the vortex glass cannot be distinguished from the vortex liquid through the breaking of any translational or orientational symmetries, but only through broken gauge symmetry, scaling procedures have been proposed to identify whether one is actually dealing with a phase transition [Fisher, Fisher, and Huse 1991]. Scaling of thermodynamic and transport properties around the vortex glass phase transition line $T_g(B)$ would expose the existence of a diverging length scale $\xi_g \propto |T - T_g|^{-\nu}$ ("the glass correlation length") describing the establishment of long-range order of the superconducting phase. The vortex glass theory predicts a specific behaviour for the resistivity in the critical regime around $T_g(B)$ where all data for different temperatures and fields collapse on two curves, F_+ for $T > T_g$ and F_- for $T < T_g$ [Koch *et al.* 1989] when plotted as $(E/j) \cdot |T - T_g|^{-\nu(z-1)}$ versus $(j/T) \cdot |T - T_g|^{-2\nu}$. Here, z is a universal dynamic exponent describing critical slowing down. A typical experimental scaling plot is shown in figure A3.2.9. The exact functional dependence of $F_\pm$ is unknown. $F_+ \to 1$ for small j denoting linear resistivity, and $F_- \to \exp(-1/x^\mu)$ for small x, describing true superconductivity. At T_g, E should depend on j according to the power law $E \propto j^{(z+1)/2}$. Although there are many reports of the observation of vortex-glass scaling, in particular in thin films of the high-T_c cuprate $YBa_2Cu_3O_{7-\delta}$, no clear consensus as to the universality of scaling has emerged. This may partially be due to the presence of extended defects such as screw dislocations cores, for which the Bose-glass approach is more suited [Nakielski *et al.* 1996].

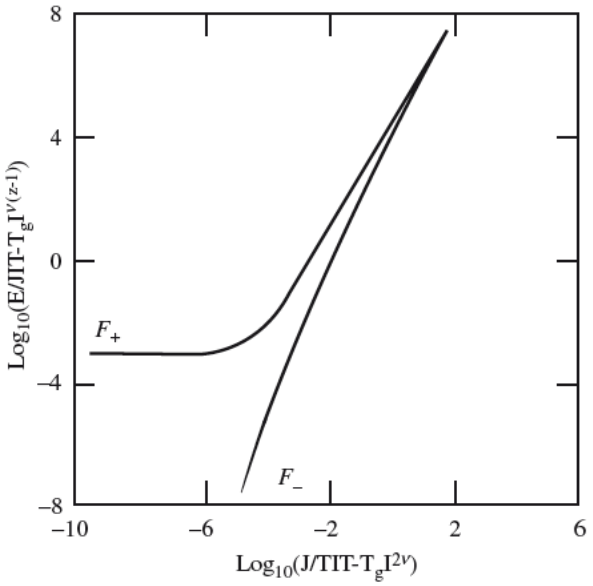

Figure A3.2.9: Collapse of over 100 I – V curves in a vortex-glass scaling plot for $YBa_2Cu_3O_7$ in a field of 4 T for the parameter values $T_g = 74.5$ K, $z = 4.8$ and $\nu = 1.7$ [Koch *et al.* 1989].

Another issue is the homogeneity of disorder. Heterogeneity of the material disorder (on various length scales) may lead to local variations of parameters such as the superconducting transition temperature and / or the superfluid density and thereby to a spatially inhomogeneous vortex glass to liquid transition [Demirdis *et al.* 2010, Demirdis *et al.* 2013]. This will appear as concomitantly broadened, when averaged physical quantities such as the resistivity or magnetic moment of the full sample are measured, compromising the verification of any hypothetical scaling laws. At the same time, the spatial inhomogeneity of disorder on the nm scale was itself shown to be a source of pinning [Demirdis *et al.* 2010, Demirdis *et al.* 2013].

A3.2.6.8 The Bose-glass to vortex liquid transition

The Bose-glass to liquid transition has a phenomenology similar to the vortex glass transition, but is distinguished by its dependence on the orientation of the sample defect structure with respect to the field direction, and by the anisotropy of the vortex dynamics. To account for this, the Bose-glass theory introduces the correlations lengths $\xi_\perp$ and $\xi_\parallel = \xi_\perp^\varsigma$ perpendicular and parallel to the linear defects, respectively [Nelson and Vinokur 1992, Lidmar and Wallin 1999]. Here ς is the anisotropy exponent. At the Bose-glass transition, the linear resistivity for field perpendicular and parallel to defects scales as

$$\rho_\perp = \frac{E_\perp}{j_\perp} \sim \xi_\perp^{D+\varsigma-z-3} \sim \left|\frac{T-T_{BG}}{T_{BG}}\right|^{\nu(2-z)} \tag{A3.2.21}$$

$$\rho_\parallel = \frac{E_\parallel}{j_\parallel} \sim \xi_\parallel^{D-\varsigma-z-1} \sim \left|\frac{T-T_{BG}}{T_{BG}}\right|^{-\nu z} \tag{A3.2.22}$$

where the last step was taken by invoking $\varsigma = 2$ and a spatial dimension $D = 3$. At the Bose-glass transition temperature, the $E(j)$–curve again shows a power-law,

$$E_\perp = j^{(1+z)/(2-D-\varsigma)} \quad \text{(A3.2.23)}$$

$$E_\parallel = j^{(\varsigma+z)/(1-D)}. \quad \text{(A3.2.24)}$$

Some experimental evidence for such scaling behaviour has been found in $YBa_2Cu_2O_{7-\delta}$, both as a result of twin-boundary pinning in single crystalline material [Grigera *et al.* 1999], and as a result of pinning by heavy-ion irradiation-induced latent tracks in both single crystals [Jiang *et al.* 1994, Espinosa *et al.* 2006] and films [Nakielski *et al.* 1996].

A3.2.6.9 Two-dimensional vortex melting

The only available complete theory [Berezinskii 1972, Kosterlitz and Thouless 1978, Nelson and Halperin 1979] for the transition from the low-temperature vortex state to the vortex liquid state describes the situation in thin superconducting films of thickness $d < L_c$, where vortex cores are straight across the thickness [Berghuis, van der Slot, and Kes 1990]. The vortex ensemble melts in two stages, accurately described by the theory of Kosterlitz-Thouless for 2D melting [Berezinskii 1972, Kosterlitz and Thouless 1978, Nelson and Halperin 1979]. In the first stage, the unbinding of vortex-lattice edge dislocation pairs in the lattice at

$$T_m^{2D} = \frac{\mathcal{A}\varepsilon_0(T_m^{2D})d}{16k_B} \qquad (b \ll 1) \quad \text{(A3.2.25)}$$

$$= \frac{\mathcal{A}\varepsilon_0(T_m^{2D})d}{16k_B}(1-b) \qquad (b \lesssim 1) \quad \text{(A3.2.26)}$$

drives the transition to a hexatic state. In the second stage, the hexatic transits to the liquid through the unbinding of disclinations (pairs of 5-fold and 7-fold coordinated vortices). At the melting line, the shear modulus should fall to zero, although in practice disorder smears out the transition.

A3.2.6.10 Plasticity of the vortex lattice and the peak effect

A sudden increase of the sustainable current density is often apparent in measurements of the irreversible magnetic moment of type-II superconductors, or in plots of j_c versus H or T. This phenomenon causes a dip in $R(T)$ or $R(H)$, while in ac-susceptibility experiments a peak in χ'' occurs each time the condition $h_0 \sim H^*$ is fulfilled. Depending on the material, this "peak effect" can occur at rather low magnetic fields, or, more often, just before the vortex glass to liquid transition. At the basis of the "peak effect" is the transition between different regimes of flux pinning, driven by the appearance of plastic deformations of the vortex ensemble [Mikitik and Brandt 2001]. This translates to an abrupt transition between (often crossing) $E(j)$–curves characterised by different curvatures and different current density scales j_c. This results, in experiment, to an abrupt change of the working point. It also means that in inductive measurements the peak can appear or disappear as function of field sweep rate, temperature, or waiting time after a field change, as the working points on the $E(j)$–curves shift. The peak effect is only observed in situations where pinning is initially weak, or of intermediate strength.

In many bulk superconductors ($d \gg L_c$) a nearly temperature–independent first–order phase transition underlies the peak effect, which therefore appears primarily on sweeping the applied magnetic field [Kokkaliaris *et al.* 1999, van der Beek *et al.* 2000, Avraham *et al.* 2001, Klein *et al.* 2010]. Neutron scattering measurements [Aragón *et al.* 2019] as well as vortex decoration experiments [Aragón *et al.* 2019] show that at the transition, the vortex ensemble changes from a rather ordered state, which may be the Bragg glass, to a vortex polycrystal. This suggests that the peak effect is triggered by the appearance of edge- and screw dislocations that allows the vortex ensemble to better adapt

to the pinning potential. The transition to the (denser) high–field disordered vortex state is driven by the gain in pinning energy, while the low–field ordered state is stabilised by the gain in elastic deformation energy and the elimination of vortex lattice dislocations. Above the depinning temperature T_{dep}, the energy gain that can be obtained from pinning decreases sharply, and the transition to the disordered state moves to higher magnetic fields, eventually joining the vortex melting transition in a tricritical point [Safar *et al.* 1993]. This fact poses the as-yet unanswered question whether the high–field disordered state is thermodynamically distinct from the vortex liquid or not.

In materials showing weak collective pinning such as α-Nb_3Ge [Wördenweber and Kes 1986], $NbSe_2$ [Koorevaar *et al.* 1990, Bhattacharya and Higgins 1993, Banerjee *et al.* 1998], $CeRu_2$ [Banerjee *et al.* 1998], MgB_2 [Klein *et al.* 2010], or $BaFe_2(As_{1-x}P_x)_2$ [Putzke *et al.* 2014], the peak effect may show only in the vicinity of the upper critical field. In such cases, it is the softening of the elastic moduli (notably c_{44}) of the vortex lattice on approaching B_{c2} that is responsible for the appearance of plastic deformations of the vortex lattice and stronger pinning. A controlled increase of the pinning strength, for example, though electron irradiation, moves the peak effect transition field down [Klein *et al.* 2010].

In two-dimensional superconducting films, the peak effect is closely associated with the two-dimensional vortex melting [Berghuis, van der Slot, and Kes 1990]. Here, it is the unbinding of vortex lattice edge dislocations pairs that allows the vortex ensemble to better adjust to the pinning potential [Wördenweber and Kes 1986].

A3.2.7 Vortex dynamics at high driving force

Even for current densities above j_c, the driven vortex ensemble is still influenced by the presence of the "quenched" pinning potential. Notably, the pinning potential induces fluctuations δv of the velocity of the moving vortex ensemble, and, more rarely, of the vortex density $\delta n_v = \delta B/\Phi_0$. These fluctuations result in a voltage noise contribution $\delta V = \overline{n}_v \delta v + \overline{v}\delta n_v$ characteristic of vortex motion [van Oijen and van Gurp 1965, Clem 1981]. Most often, the voltage noise is related to the (irregularity of the) entrance and exit of vortex lines [Paltiel *et al.* 2000]; its frequency spectrum is therefore related to the (spectrum of) vortex transit time(s) through the sample. However, it has been shown that both the magnitude of the noise and the spectrum are also clearly affected by flux pinning in the superconductor, and depend on the strength of pinning in the superconductor and the ensuing positional order of the vortex ensemble. Most prominently, edge-induced vortex lattice disorder (see subsection *A3.2.3.8*) and subsequent annealing at high driving forces have been shown to be directly linked to the noise spectrum [Paltiel *et al.* 2004].

Strong pinning is prone to lead to more pronounced flux density gradients associated with the drive current, and, thereby, to the associated avalanche-like motion of the vortex ensemble. These occur on time scales smaller than the transit time and have been suggested to result in $1/f$–noise [Bak, Tang, and Wiesenfeld 1987, Altshuler and Johansen 2004]. It has been shown that the $1/f$ noise ubiquitous in strongly pinning high temperature superconducting films and devices can be effectively suppressed by the appropriate incorporation of artificial pinning structures [Wördenweber, Castellanos, and Selders 2000].

When pinning is weak, vortex motion is more regular. In this case, the quasi-periodic nature of the moving Bragg glass entails the motion of vortices in well-ordered rows [Giamarchi and Le Doussal 1996]. In this scenario, each vortex line encounters the same disorder configuration and undergoes the same depinning events as its predecessors, which leads to the appearance of a so-called "washboard frequency" $f_w = v/a_0$ and narrow-band noise [Pardo *et al.* 1998, Troyanovsky, Aarts, and Kes 1999, Togawa *et al.* 2000]. The presence of these spectral features may appear as a distinguishing feature between the different vortex phases outlined above [Togawa *et al.* 2000].

Bibliography

[Altshuler and Johansen 2004] Altshuler E and Johansen T H (2004) Experiments in vortex avalanches, Reviews of Modern Physics 76: 471

[Aragón *et al.* 2019] Aragón Sánchez J *et al.* (2019) Unveiling the vortex glass phase in the surface and volume of a type-II superconductor, Nature Communications Physics 2: 143

[Avraham *et al.* 2001] Avraham N *et al.* (2001) 'Inverse' melting of a vortex lattice, Nature (London) 411: 451

[Bak, Tang, and Wiesenfeld 1987] Bak P, Tang C, and Wiesenfeld K (1986) Self-organised criticality: and explanation of $1/f$ noise, Phys. Rev. Lett. 59: 381

[Banerjee *et al.* 1998] Banerjee S S *et al.* (1998) Anomalous peak effect in $CeRu_2$ and 2H–$NbSe_2$: Fracturing of a flux line lattice, Phys. Rev. B 58(2):995-999

[Bardeen and Stephen 1965] Bardeen J and Stephen M J (1965) Theory of the Motion of Vortices in Superconductors Phys. Rev. 140 : A1197

[Bartolomé *et al.* 2019] Bartolomé E, Vallés F, Palau A, Rouco V, Pompeo N, Balakirev F F, Maiorov B, Civale L, Puig T, Obradors X, and Silva E (2019) Intrinsic anisotropy versus effective pinning anisotropy in $YBa_2Cu_3O_7$ thin films and nanocomposites, Phys. Rev. B 100: 054502

[Bean 1962] Bean C P (1962) Magnetization of hard superconductors Phys. Rev. Lett. 8: 250

[van der Beek *et al.* 1992] van der Beek C J, Kes P H, Maley M P, Menken M J V and Menovsky A A (1992) Flux pinning and creep in the vortex-glass phase in $Bi_2Sr_2CaCu_2O_{8+\delta}$ single crystals Physica C 195: 307

[van der Beek *et al.* 1996] C.J. van der Beek, M.V. Indenbom, G. D'Anna, and W. Benoit (1996) Physica C 258: 105

[van der Beek *et al.* 1996] van der Beek C J, Konczykowski M, Li T W, Kes P H and Benoit W (1996) Large effect of columnar defects on the thermodynamic properties of $Bi_2Sr_2CaCu_2O_8$ single crystals Phys. Rev. B 54: R792

[van der Beek *et al.* 1996] van der Beek C J, Indenbom M V, Berseth V, Li T W and Benoit W (1996) Onset of bulk pinning in BSCCO single crystals, J. Low. Temp. Phys. 105: 1047

[van der Beek *et al.* 2000] van der Beek C J, Colson S, Indenbom M V, and Konczykowski M (2000) Supercooling of the disordered vortex lattice in $Bi_2Sr_2CaCu_2O_8$, Phys. Rev. Lett. 84: 4196.

[van der Beek *et al.* 2002] van der Beek C J *et al.* (2002) Strong pinning in high temperature superconducting films Phys. Rev. B 66: 024523

[van der Beek *et al.* 2005] van der Beek C J *et al.* (2005) Thermodynamics of the vortex liquid in heavy-ion-irradiated superconductors, Phys. Rev. B 72: 214504

[van der Beek *et al.* 2010] van der Beek C J *et al.* (2010) Quasiparticle scattering induced by charge doping of iron-pnictide superconductors probed by collective vortex pinning Phys. Rev. Lett. 105: 267002

[Berezinskii 1972] Berezinskii V L (1972) Destruction of Long-range Order in One-dimensional and Two-dimensional Systems Possessing a Continuous Symmetry Group, Sov. Phys. JETP **34** 610

[Berghuis, van der Slot, and Kes 1990] Berghuis P, van der Slot A L F, and Kes P H (1990) Dislocation-mediated vortex-lattice melting in thin films of α-Nb_3Ge Phys. Rev. Lett. 65: 2583

[Bhattacharya and Higgins 1993] Bhattacharya S and Higgins M J (1993) Dynamics of a disordered flux line lattice, Phys. Rev. Lett. 70: 2617

[Blatter *et al.* 1994] Blatter G, Feigel'man M V, Geshkenbein V B, Larkin A I and Vinokur V M 1994 Vortices in high-temperature superconductors Rev. Mod. Phys. 66: 1125

[Blatter, Geshkenbein, and Koopman 2004] Blatter J, Geshkenbein V B, and Koopman J A G (2004) Weak to strong pinning crossover Phys. Rev. Lett. 92: 067009

[Bourgault *et al.* 1989] Bourgault D, Groult D, Bouffard S, Provost J, Studer F, Nguyen N, Raveau B, and Toulemonde M (1989) Modifications of the physical properties of the high-T_c superconductors $YBa_2Cu_3O_{7-\delta}$ ($0.1 \leq \delta < 0.7$) by 3.5-GeV xenon ion bombardment, Phys. Rev. B 39: 6549 (1989)

[Brandt 1989] Brandt E H (1989) Thermal fluctuation and melting of the vortex lattice in oxide superconductors, Phys. Rev. Lett. 63: 1106

[Brandt 1996] Brandt E H (1996) Superconductors of finite thickness in a perpendicular magnetic field: Strips and slabs Phys. Rev. B 54: 4246

[Brandt 2003] Brandt E H (2003) Properties of the ideal Ginzburg-Landau vortex lattice, Phys. Rev. B 68: 054506

[Brézin, Nelson, and Thiaville 1985] Brézin E, Nelsonn D R, and Thiaville A (1985) Fluctuation effects near H_{c2} in type-II superconductors, Phys. Rev. B 31: 7124

[Campbell and Evetts 1972] Campbell A M and Evetts J E (1972) Flux vortices and transport currents in type II superconductors Adv. Phys. 21: 199

[Civale *et al.* 1991] Civale L, Marwick A D, Worthington T K, Kirk M A, Thompson J R, Krusin-Elbaum L, Sun Y, Clem J R, and Holtzberg FF (1991) Vortex confinement by columnar defects in $YBa_2Cu_3O_7$ crystals: Enhanced pinning at high fields and temperatures, Phys. Rev. Lett. 67: 648

[Clem 1974] Clem J, (1974) A model for flux pinning in superconductors Low Temperature Physics LT-13 3, eds K D Timmerhaus, W J O'Sullivan and E F Hammel (Plenum: New York) p 102

[Clem 1981] Clem J R (1981) Flux-flow noise in superconductors, Physics Reports 75(1): 1-55

[Clem and Sanchez 1994] Clem J R and Sanchez A (1994) Hysteretic ac losses of thin superconducting disks Phys. Rev. B 50: 9355

[Demirdis *et al.* 2010] Demirdis S *et al.* (2011) Strong pinning and vortex energy distributions in single-crystalline $Ba(Fe_{1-x}Co_x)_2As_2$ Phys. Rev. B 84: 094517

[Demirdis *et al.* 2013] Demirdiş *et al.* (2013) Disorder, critical currents, and vortex pinning energies in isovalently substituted $BaFe_2(As_{1-x}P_x)_2$ " Phys Rev. B 87: 094506

[de Gennes 1989] de Gennes P G (1989) Superconductivity of Metals and Alloys, p. 83 (Addison Wesley, New York)

[Edwards and Wilkinson 1982] Edwards S F and Wilkinson D R (1982) The Surface Statistics of a Granular Aggregate. Proc. R. Soc. Lond. Ser. A 381: 17

[Espinosa *et al.* 2006] Espinosa-Arronte B, Andersson M, van der Beek C J, Nikolaou M, Lidmar J, and Wallin M 2007 Fully anisotropic superconducting transition in ion-irradiated $YBa_2Cu_3O_{7-\delta}$ with a tilted magnetic field, Phys. Rev. B 75: 100504(R)

[Feigel'man and Vinokur 1990] Feigel'man M V and Vinokur V M (1990) Thermal fluctuations of vortex lines, pinning and creep in high-T_c superconductors, Phys. Rev. B 41: 8986

[Feigel'man *et al.* 1989] Feigel'man M V, Geshkenbein V B, Larkin A I, and Vinokur V M (1989) Theory of collective flux creep Phys. Rev. Lett. 63: 2303

[Fendrich *et al.* 1995] Fendrich J A *et al.*(1995) Vortex Liquid State in an Electron Irradiated Untwinned $YBa_2Cu_3O_{7-\delta}$ Crystal, Phys. Rev. Lett. 74: 1210

[Fisher, Fisher, and Huse 1991] Fisher D S, Fisher M P A, and Huse D (1991) Thermal fluctuations, quenched disorder, phase transitions and transport in type II superconductors Phys. Rev. B 43: 130

[Fuchs *et al.* 1998] Fuchs D T, Zeldov E, Tamegai T, Ooi S, Rappaport M and Shtrikman H (1998) Possible new vortex matter in $Bi_2Sr_2CaCu_2O_8$, Phys. Rev. Lett. 80: 4971

[Giamarchi and Le Doussal 1994] Giamarchi T and Le Doussal P (1994) Elastic theory of pinned flux lattices Phys. Rev. Lett. 72: 1530

[Giamarchi and Le Doussal 1995] Giamarchi T and Le Doussal P (1995) Elastic theory of flux lattices in the presence of weak disorder Phys. Rev. B 52:1242

[Giamarchi and Le Doussal 1996] Giamarchi, T and Le Doussal P (1996) Moving glass phase of driven lattices. Phys. Rev. Lett. 76 : 3408

[Grigera *et al.* 1999] Grigera S, Morré E, Osquiguil E, Balseiro C, Nieva G, de la Cruze F (1998) Bose-Glass Phase in Twinned $YBa_2Cu_3O_{7-\delta}$, Phys. Rev. Lett. 81: 2348

[Grisolia2013] Grisolia M N, van der Beek C J, Fasano Y, Forget A and Colson D (2013) Multifractal scaling of flux penetration in the iron-based superconductor $Ba(Fe_{0.93}Co_{0.07})_2As_2$ Phys. Rev. B 87: 104517

[Indenbom 1995] Indenbom M V, Schuster Th, Kuhn H, Kronmüller H, Li T W, and Menovsky A A (1995) Observation of current strings in $Bi_2Sr_2CaCu_2O_8$ single crystals Phys. Rev. B 51: 15484

[Imry and Ma 1975] Imry Y and Ma S-K (1975) Random-Field Instability of the Ordered State of Continuous Symmetry Phys. Rev. Lett. 35: 1399

[Indenbom *et al.* 1994] Indenbom M V, Kronmüller H, Li T W, Kes P H, and Menovsky A A (1994) Equilibrium magnetic properties and Meissner expulsion of magnetic flux in $Bi_2Sr_2CaCu_2O_x$ single crystals Physica(Amsterdam) C 222: 203

[Jiang *et al.* 1994] Jiang W *et al.* (1994), Evidence of a Bose-glass transition in superconducting $YBa_2Cu_3O_{7-\delta}$ single crystals with columnar defects, Phys. Rev. Lett. 72: 550

[Kes *et al.* 1989] Kes P H, Aarts J, Van den Berg J, Van der Beek C J and Mydosh J A (1989) Thermally assisted flux flow at small driving forces Supercond Sci. Technol. 1: 242

[Kes 1992] Kes P H (1992) Flux pinning and the summation of pinning forces. In: Concise Encyclopedia of Magnetic & Superconducting Materials (J E Evetts ed.) p 163. Oxford: Pergamon

[Kim *et al.* 1998] Kim P, Yao Z, Bolle C A, Lieber C M (1999) Structure of flux line lattices with weak disorder at large length scales Phys. Rev. B 60: 12589

[Klein *et al.* 2010] Klein T *et al.* (2010) First-Order Transition in the Magnetic Vortex Matter in Superconducting MgB_2 Tuned by Disorder, Phys. Rev. Lett. 105: 047001

[Koch *et al.* 1989] Koch R H, Foglietti V, Gallagher W J, Koren G, Gupta A and Fisher M P A (1989) Experimental evidence for vortex-glass superconductivity in Y–Ba–Cu–O Phys. Rev. Lett. 63: 1115 ; Koch R H, Foglietti V, and Fisher M P A (1990) Reply to Comment on Experimental evidence for vortex-glass superconductivity in Y–Ba–Cu–O eds Coppersmith S N, Inui M and Littlewood P B, Phys. Lett. 64: 2586

[Kokkaliaris *et al.* 1999] Kokkaliaris S, de Groot P A J, Gordeev S N, Zhukov A A, Gagnon R, and L. Taillefer L (1999) Onset of Plasticity and Hardening of the Hysteretic Response in the Vortex System of $YBa_2Cu_3O_{7-\delta}$, Phys. Rev. Lett. 82: 5116

[Koorevaar *et al.* 1990] Koorevaar P, Aarts J, Berghuis P, and Kes P H (1990) Tilt-modulus enhancement of the vortex lattice in the layered superconductor 2H-$NbSe_2$, Phys. Rev. B 42: 1004

[Koshelev and Vinokur 1990] Koshelev A E and Vinokur V M (1991) Physica C 175: 465

[Kosterlitz and Thouless 1978] Kosterlitz J M and Thouless D J (1978) Two-dimensional physics. In Progress in Low Temperature Physics(D F Brewer ed.), vol. VII-B, pp371-433 (North-Holland, Amsterdam)

[Kwok *et al.* 1991] Kwok W K, Welp U, Vinokur V M, Fleshler S, Downey J, and Crabtree G W (1991) Direct observation of intrinsic pinning by layered structure in single-crystal $YBa_2Cu_3O_{7-\delta}$, Phys. Rev. Lett. 67: 390

[Kwok *et al.* 1992] Kwok W K, Fleshler S, Welp U, Vinokur V M, Downney J, Crabtree G W, and Miller M M (1992) Vortex lattice melting in untwinned and twinned single crystals of $YBa_2Cu_3O_{7-\delta}$, Phys. Rev. Lett. 69: 3370

[Larkin and Ovchinnikov 1979] Larkin A I and Ovchinnikov Yu N 1979 Pinning in type II superconductors J. Low Temp. Phys. 34: 409

[Li *et al.* 1996] Li T W, Menovsky A A, Franse J J M and Kes P H (1996) Flux pinning in Bi-2212 single crystals with various oxygen contents, Physica C 257: 179

[Lidmar and Wallin 1999] Lidmar J and Wallin M 1999 Critical properties of Bose-glass superconductors, Europhys. Lett. 47: 494

[López 1996] López D, Righi E F, Nieva G, de la Cruz F (1996) Coincidence of Vortex-Lattice Melting and Loss of Vortex Correlation along the c Direction in Untwinned $YBa_2Cu_3O_{7-\delta}$ Single Crystals, Phys. Rev. Lett. 76: 4034

[López *et al.* 1997] López D *et al.* (1997) Pinned Vortex Liquid above the Critical Point of the First-Order Melting Transition: A Consequence of Pointlike Disorder, Phys. Rev. Lett. 80: 1070

[Marchiori *et al.* 2017] Marchiori E, Curran P J, Kim J, Satchell N, Burnell G, and Bending S J (2017) Reconfigurable superconducting vortex pinning potential for magnetic disks in hybrid structures, Scientific Reports 7: 45182

[Mele *et al.* 2019] Mele P, Prassides K, Tarantini C, Palau A, Badica P, Jha A K, Endo T (2019) Superconductivity: From Materials Science to Practical Applications. Springer Nature ISBN-13 978-3030233020

[Mikitik and Brandt 2001] Mikitik G P and Brandt E H (2001) Peak effect, vortex-lattice melting line, and order-disorder transition in conventional and high-T_c superconductors, Phys. Rev. B 64: 184514

[Nakielski *et al.* 1996] Nakielski G *et al.* (1996) Enhancement of Bose-Glass Superconductivity in $YBa_2Cu_3O_{7-\delta}$ Thin Films, Phys. Rev. Lett. 76: 2567

[Nelson and Halperin 1979] Nelson D R and Halperin B I (1979) Dislocation-mediated melting in two dimensions, Physical Review B. 19: 2457.

[Nelson and Vinokur 1992] Nelson D R and Vinokur V M (1992) Boson localization and pinning by correlated disorder in high-temperature superconductors, Phys Rev Lett. 68: 2398 ; Phys. Rev. B 48: 13060

[van Oijen and van Gurp 1965] van Ooijen D J and van Gurp G J (1965) Motion and pinning of fluxin superconducting vanadium foils, studied by means of noise, Phys. Letters, 17: 230.

[Ovchinnikov and Ivlev 1991] Ovchinnikov Yu N and Ivlev B I (1991) Pinning in layered inhomogeneous superconductors Phys. Rev. B 43: 8024

[Paltiel *et al.* 2000] Paltiel Y *et al.* (2000) Dynamic instabilities and memory effects in vortex matter Nature 403: 398–401

[Paltiel *et al.* 2004] Paltiel Y, Jung G, Myasoedov Y, Rappaport M L, Zeldov E, Ocio M, Higgins M J , and Bhattacharya S (2004) Velocity-fluctuations–dominated flux-flow noise in the peak effect, Europhys. Lett., 66 (3): 412

[Pardo *et al.* 1998] Pardo F, de la Cruz F, Gammel P L, Bucher E and Bishop D J (1998) Observation of smectic and moving-Bragg-glass phases in flowing vortex lattices, Nature 396 : 348–350

[Putzke *et al.* 2014] Putzke C *et al.* (2014) Anomalous critical fields in quantum critical superconductors, Nature Communications 5: 5679

[Sadovskyy *et al.* 2015] Sadovskyy I A, Koshelev A E, Glatz A, Ortalan V, Rupich M W, Leroux M (2015) Simulation of the vortex dynamics in a real pinning landscape of $YBa_2Cu_3O_{7-\delta}$ coated conductors, Phys. Rev. Applied 5: 014011

[Safar *et al.* 1992] Safar H, Gammel P L, Huse D A, Bishop D J, Rice J P, and Ginsberg D M (1992) Experimental evidence for a first-order vortex-lattice-melting transition in untwinned, single crystal $YBa_2Cu_3O_{7-\delta}$, Phys. Rev. Lett. 69: 824

[Safar *et al.* 1993] Safar H *et al.* (1993) Experimental evidence for a multicritical point in the magnetic phase diagram for the mixed state of clean untwinned $YBa_2Cu_3O_{7-\delta}$, Phys. Rev. Lett. 70: 3800

[Schilling *et al.* 1996] Schilling A *et al.* (1996) Calorimetric measurement of the latent heat of vortex-lattice melting in untwinned $YBa_2Cu_3O_{7-\delta}$, Nature 382 (6594): 791

[Schuster *et al.* 1994] Schuster Th, Indenbom M V, Kuhn H, Kronmüller H, Leghissa M, and Kreiselmeyer G (1994) Observation of in-plane anisotropy of vortex pinning by inclined columnar defects, Phys. Rev. B 50: 9499

[Thompson *et al.* 1997] Thompson J R, Krusin-Elbaum L, Civale L, Blatter G and Feild C (1998) Superfast Vortex Creep in $YBa_2Cu_3O_{7-\delta}$ Crystals with Columnar Defects: Evidence for Variable-Range Vortex Hopping, Phys. Rev . Lett. 78: 3181

[Togawa *et al.* 2000] Togawa Y, Abiru R, Iwaya K, Kitano H, Maeda A (2000) Direct observation of the washboard noise of a driven vortex lattice in a high-temperature superconductor, $Bi_2Sr_2CaCu_2O_y$, Phys Rev Lett. 85(17): 3716-9.

[Troyanovsky, Aarts, and Kes 1999] Troyanovsky A M, Aarts J, Kes P H (1999) Collective and plastic vortex motion in superconductors at high flux densities, Nature 399 : 665

[Wördenweber and Kes 1986] Wördenweber R, Kes P H and Tsuei C C (1986) Peak and history effects in two-dimensional collective flux pinning Phys. Rev. B 33: 3172

[Wördenweber and Kes 1986] Wördenweber R and Kes P H (1986) Dimensional crossover in collective flux pinning, Phys. Rev. B 34: 494(R)

[Wördenweber, Castellanos, and Selders 2000] Wördenweber R, Castellanos A M, and Selders P (2000) Vortex lattice matching effects and $1/f$-noise reduction in HTS films and devices equipped with regular arrays of artificial defects, Physica C: Superconductivity 332 (1–4): 27-34

[Zeldov *et al.* 1994] Zeldov E *et al.* (1994) Geometrical barriers in high temperature superconductors Phys. Rev. Lett. 73: 1428

[Zeldov *et al.* 1995] Zeldov E, Majer D, Konczykowski M, Geshkenbein V B, Vinokur V M and Shtrikman H (1995) Thermodynamic observation of first-order vortex-lattice melting in $Bi_2Sr_2CaCu_2O_8$ Nature 375: 373